CSF-1 maintains pathogenic but not homeostatic myeloid cells in the central nervous system during autoimmune neuroinflammation.

Daniel Hwang[1], Maryam S. Seyedsadr[1], Larissa Lumi Watanabe Ishikawa[1], Alexandra Boehm[1], Ziver Sahin[1], Giacomo Casella[1], Soohwa Jang[1], Michael V. Gonzalez[2], James P. Garifallou[2], Hakon Hakonarson[2,3], Weifeng Zhang[1], Dan Xiao[1], Abdolmohamad Rostami[1], Guang-Xian Zhang[1], and Bogoljub Ciric[1,*]

[1]Department of Neurology, Jefferson Hospital for Neuroscience, Thomas Jefferson University, Philadelphia, PA.

[2]Center for Applied Genomics, The Children's Hospital of Philadelphia, Abramson Research Center, Philadelphia, PA, 19104.

[3]Department of Pediatrics, Perelman School of Medicine, University of Pennsylvania, Philadelphia PA, 19104

*Corresponding author: Bogoljub Ciric, Ph.D., Associate Professor, Department of Neurology, Jefferson Hospital for Neuroscience, Thomas Jefferson University, 900 Walnut Street, Suite 300, Philadelphia, PA, 19107. bogoljub.ciric@jefferson.edu

Short title: Blocking CSF-1 ameliorates EAE.

ABSTRACT

The receptor for colony stimulating factor 1 (CSF-1R) is important for the survival and function of myeloid cells that mediate pathology during experimental autoimmune encephalomyelitis (EAE), an animal model of multiple sclerosis (MS). CSF-1 and IL-34, the ligands of CSF-1R, have similar bioactivities but distinct tissue and context-dependent expression patterns, suggesting that they have different roles. This could be the case in EAE, given that CSF-1 expression is upregulated in the CNS, while IL-34 remains constitutively expressed. We found that targeting CSF-1 with neutralizing mAb halted ongoing EAE, with efficacy superior to CSF-1R inhibitor BLZ945, whereas IL-34 neutralization had no effect, suggesting that pathogenic myeloid cells were maintained by CSF-1, not IL-34. Both anti-CSF-1- and BLZ945-treatment greatly reduced numbers of monocyte-derived cells and microglia in the CNS. However, anti-CSF-1 selectively depleted inflammatory microglia and monocytes in inflamed CNS areas, whereas BLZ945 depleted virtually all myeloid cells, including quiescent microglia, throughout the CNS. Anti-CSF-1 treatments reduced the size of demyelinated lesions, and microglial activation in the grey matter. Lastly, we found that bone marrow-derived immune cells were the major mediators of CSF-1R-dependent pathology, while microglia played a lesser role. Our findings suggest that targeting CSF-1 could be effective in ameliorating MS pathology, while preserving the homeostatic functions of myeloid cells, thereby minimizing risks associated with total ablation of CSF-1R-dependent cells.

Significance Statement

Multiple sclerosis (MS) and its animal model, experimental autoimmune encephalomyelitis (EAE), are autoimmune diseases characterized by accumulation of myeloid immune cells into the central nervous system (CNS). Both harmful and beneficial myeloid cells are present in EAE/MS, and a goal of MS therapy is to preferentially remove harmful myeloid cells. The receptor for CSF-1 (CSF-1R) is found on myeloid cells and it is important for their survival. CSF-1R can bind two ligands, CSF-1 and IL-34, but is unknown whether their functions in EAE/MS differ. We found that blocking CSF-1 depleted only harmful myeloid cells in the CNS and suppressed EAE, whereas blocking IL-34 had no effect. Thus, we propose that blocking CSF-1 could be a novel therapy for MS.

INTRODUCTION

Multiple sclerosis (MS) is an autoimmune disease characterized by accumulation of immune cells in inflamed areas of the central nervous system (CNS), which eventually become demyelinated lesions [2]. Myeloid cells account for up to 85% of immune cells in active MS lesions [3-5], suggesting that they are the major mediators of pathology in MS. In support of this notion, studies in experimental autoimmune encephalomyelitis (EAE), an animal model of MS, have demonstrated the essential role of myeloid cells in EAE pathology, as interventions that affect them, in particular monocytes and conventional dendritic cells (cDCs), ameliorate or abrogate EAE [6-8]. However, despite evidence on the importance of myeloid cells in CNS autoimmunity, they have not been specifically targeted for MS therapy. This provides an opportunity for devising therapeutic approaches that target myeloid cells relevant to MS pathology.

Receptor for colony stimulating factor 1 (CSF-1R) is a cell-surface receptor tyrosine kinase that binds two ligands, CSF-1 (a.k.a. M-CSF) and IL-34 [9]. CSF-1R signaling facilitates survival and proliferation of myeloid cells, with either CSF-1 or IL-34 predominantly controlling the population size of myeloid cells in various organs and tissues [9-11]. CSF-1R is expressed by microglia, monocytes and monocyte-derived cells, which comprise the bulk of myeloid cells in the CNS during MS and EAE [10]. CSF-1R function is not intrinsically pro-inflammatory, as CSF-1R signaling in steady state induces a regulatory/homeostatic phenotype in macrophages, and a resting/quiescent phenotype in microglia [1, 12-26]. However, in inflammation, CSF-1R function could indirectly be pro-inflammatory, by simply perpetuating the survival and expansion of inflammatory myeloid cells. A recent study found an increase in both CSF-1R and CSF-1 in and around demyelinating lesions in cortical white matter of patients with progressive MS, and elevated CSF-1 in patients' cerebrospinal fluid, whereas IL-34 was not increased, suggesting that CSF-1 drives the deleterious role of CSF-1R in MS [27]. In the progressive EAE model, CSF-1R has been identified as a key regulator of the inflammatory response in the CNS, with CSF-1R and CSF-1 expression levels correlating with disease progression. Inhibition of CSF-1R with small molecule inhibitor reduced the expression of pro-inflammatory genes and restored expression of homeostatic genes in microglia of mice with EAE [27].

It has been shown that direct inhibition of CSF-1R kinase activity with small molecule inhibitors suppresses EAE pathology [28, 29], but the effects of CSF-1R inhibition on particular cell subsets remain poorly understood. Different methods for reducing CSF-1R signaling, such as by antibodies (Ab) against the receptor or its individual ligands, have not been compared with small molecule inhibitors. The principal difference between these blocking methods is that small molecule inhibitors readily penetrate the entire CNS [1], whereas Abs have limited access, mainly to inflamed areas where the blood-brain barrier (BBB) has been compromised [10, 30]. Further, inhibitors of CSF-1R kinase activity could also affect other kinases [31], causing unwanted effects, especially over their prolonged use for therapy. In addition, direct inhibition of CSF-1R indiscriminately affects its systemic functions in their entirety, whereas individual neutralization of CSF-1 and IL-34 would have more nuanced effects, by preserving functions of the ligand that has not been targeted. These differences could lead to distinct outcomes in therapy of autoimmune neuroinflammation, given that the types and numbers of myeloid cells affected by various means of CSF-1R inhibition can substantially differ. In addition, any indirect effects of CSF-1R inhibition on cells that do not express CSF-1R also remain largely uncharacterized.

Our data and other studies show that small molecule inhibitors of CSF-1R cause a profound depletion of microglia [1, 10], which may be an important drawback in their use for therapy, as microglia play important roles in CNS homeostasis [23]. It has also been shown that neurons can express CSF-1R during excitotoxic injury, contributing to their survival [23]. Notably, it remains unknown whether neurons express CSF-1R in EAE and MS, and if its expression would be of significance, but, if so, restricting inhibition of CSF-1R signaling to inflamed areas of the CNS could be beneficial for neuronal survival. Thus, the ideal MS therapy would preferentially block CSF-1R signaling only in inflamed regions, affecting only inflammatory myeloid cells in them, while sparing cells in the rest of the CNS, such as quiescent microglia. This may be accomplished by targeting CSF-1R ligands, CSF-1 and IL-34, which show spatial- and context-dependent differences in expression [32]. Notably, although some minor differences have been described [33], CSF-1 and IL-34 have similar functions at the cellular level [34], suggesting that the differences found in animals lacking CSF-1 or IL-34 are primarily due to differential expression patterns [35]. IL-34 also binds to a second receptor, PTP-ζ [36], which has functions in oligodendrocyte development and homeostasis [37]. CSF-1 is systemically the dominant CSF-1R ligand, with its serum concentrations approximately ten times greater than that of IL-34 [15, 38-43]. Importantly, CSF-1 is not highly expressed in the CNS, but its expression can be upregulated by inflammation or injury [44], facilitating

106 expansion of myeloid cells at the site of inflammation. In contrast to more widespread CSF-1 expression, IL-34
107 is primarily and constitutively expressed in the CNS and skin [45, 46]. In steady state, IL-34 maintains survival
108 of tissue-resident myeloid cells in the skin and CNS, as the primary effect of IL-34 knockout is lack of Langerhan's
109 cells and microglia, respectively [32]. IL-34 is the predominant CSF-1R ligand in the CNS, accounting for 70%
110 of total CSF-1R signaling in healthy brain [23].

111 In the present study, we sought to understand how CSF-1R inhibition affects immune cells in the CNS of
112 mice with EAE, and to determine how the effects of blocking CSF-1 and IL-34 may differ from blocking CSF-1R.
113 We found that treatment with CSF-1R inhibitor BLZ945 suppresses EAE when given both prophylactically and
114 therapeutically. Treatment efficacy correlated with a dramatic reduction in the numbers of monocytes, monocyte-
115 derived dendritic cells (moDCs), and microglia, suggesting that loss of one or more of these cell types is
116 responsible for EAE suppression. We also found that blockade of CSF-1, but not of IL-34, with Ab suppressed
117 EAE. Importantly, anti-CSF-1 treatment preferentially depleted inflammatory myeloid cells, whereas quiescent
118 microglia were preserved. These findings suggest that blocking CSF-1, rather than CSF-1R, may be a suprerior
119 therapeutic strategy for alleviating pathology in MS.

120

121

122

123

124

125

126

127

128

129

130

131 **RESULTS**

132 **Blocking CSF-1R or CSF-1, but not IL-34, suppresses EAE.**

133 To determine the roles of CSF-1R, CSF-1, and IL-34 in EAE, we blocked them with either a small-
134 molecule inhibitor or neutralizing monoclonal Abs (MAbs). We blocked CSF-1R kinase function with BLZ945, a
135 CNS-penetrant small-molecule inhibitor that, among other effects, potently depletes microglia within several days
136 [1]. Treatment with BLZ945 delayed the onset of EAE for 6-15 days when given prophylactically (Fig. 1A) and
137 initially suppressed disease severity but could not halt disease progression despite continuous treatment. We
138 also blocked CSF-1R activity with neutralizing MAb, which was less effective than BLZ945 in delaying EAE onset,
139 and reducing disease severity (Fig. 1B). Surprisingly, anti-CSF-1R MAb (clone AFS98) failed to bind to microglia,
140 as determined by flow cytometry, whereas it bound to monocytes (Supplemental Fig. 1A). It is unclear why this
141 MAb did not bind to microglia, and how that may have impacted its effect in EAE.

142 We then tested how blocking either CSF-1 or IL-34 with MAbs would affect EAE. In contrast to blocking
143 CSF-1R, blocking of CSF-1 did not delay onset of disease (Fig. 1C), but did continuously suppress disease
144 severity over the course of treatment, including for over 40 days (Fig. 3B). Anti-IL-34 treatment did not suppress
145 EAE (Fig. 1D). We tested whether our treatments with the MAbs, which were rat IgGs, induced an anti-rat IgG
146 response in mice with EAE. Anti-CSF1, and control rat IgG2a isotype MAb induced similar low titers of anti-rat
147 IgG, whereas anti-CSF-1R and anti-IL-34 MAbs (both rat IgG2a) induced notably higher anti-rat IgG response
148 (Supplemental Fig. 1B), indicating that anti-rat IgG responses in treated mice may have reduced the neutralizing
149 effects of injected MAbs in the case of anti-CSF-1R and anti-IL-34 MAbs. To minimize the development of anti-
150 rat IgG responses, we treated mice with anti-IL-34 MAb immediately after the onset of clinical disease; however,
151 this treatment had no impact on disease (Supplemental Fig. 1C). We also tested whether administration of
152 recombinant CSF-1 could exacerbate EAE pathology, but i.p. injections of CSF-1 did not worsen disease
153 (Supplemental Fig. 1D). Overall, these data show that blocking CSF-1R signaling attenuates EAE, and that CSF-
154 1, but not IL-34, is the relevant CSF-1R ligand for EAE pathology.

155

156

157

158 **Inhibition of CSF-1R signaling depletes myeloid APCs in the CNS during EAE.**

159 We characterized how prophylactic treatment with BLZ945 influenced CNS inflammation at the peak of
160 EAE. BLZ945-treated animals had ~90% reduced numbers of $CD45^{+}$ cells in the CNS compared to vehicle-
161 treated animals (Fig. 2A). All major types of immune cells were reduced in number, but $CD11b^{+}$ cells were most
162 impacted, including profound depletion of $CD45^{Low}CD11b^{+}Tmem119^{+}CX3CR1^{Hi}$ microglia and
163 $CD45^{Hi}CD11b^{+}CD11c^{+}$ myeloid DCs, including $CD45^{Hi}CD11b^{+}CD11c^{+}Ly6G^{Low/-}Ly6C^{Hi}MHCII^{Hi}$ moDCs
164 (Supplemental Fig. 2). We clustered flow cytometry data by *t*-stochastic neighbor embedding (*t*-SNE) and
165 consistent with manual gating, the frequency of microglia and moDCs/macrophages was dramatically reduced
166 (Fig. 2B-E). In contrast, the frequency of neutrophils was increased; likely reflecting that they do not express
167 CSF-1R [47], and are therefore not impacted by CSF-1R inhibition. Interestingly, the frequency of
168 undifferentiated monocytes ($CD45^{Hi}CD11b^{+}Ly6C^{Hi}CD11c^{-}MHCII^{-}$) increased, suggesting that CSF-1R may
169 impact monocyte differentiation or their survival/proliferation after initial differentiation. Overall, BLZ945 treatment
170 markedly reduced the frequency of $CD11c^{+}$ myeloid antigen-presenting cells (APCs) expressing MHC class II,
171 CD80 and CD86 (Fig. 2E,F), suggesting that CSF-1R signaling maintains sufficient numbers of APCs in the CNS
172 to drive inflammation during EAE. Lastly, we found differences in cytokine production by $CD4^{+}$ T cells from
173 BLZ945-treated mice, including lower frequency of GM-CSF^{+} cells (Supplemental Fig. 2G).

174 We next tested BLZ945-treatment during ongoing EAE, as that scenario is the most relevant to MS
175 therapy. Therapeutic treatment with 200mg/kg/day BLZ945 suppressed clinical EAE, with better efficacy being
176 observed at 300 mg/kg/day (Supplemental Fig 3A-B). To determine the acute effects of CSF-1R inhibition on
177 immune cells in the CNS, we focused our analysis on mice treated with BLZ945 for 6 days, starting at a clinical
178 score of 2.0. BLZ945-treated mice had reduced numbers of $CD45^{+}$ cells in the CNS, primarily due to fewer
179 $CD11b^{+}$ and $CD11c^{+}$ cells, including microglia and $CD45^{Hi}CD11b^{+}CD11c^{+}$ myeloid DCs (Supplemental Fig. 3C-
180 F). Most immune cells depleted by BLZ945 treatment co-expressed CD11c, TNF, MHCII, CD80, and CD86,
181 suggesting that inflammatory APCs are preferentially affected by CSF-1R inhibition (Supplemental Fig. 3G-I).
182 Taken together, these data further indicate that inhibition of CSF-1R signaling suppresses EAE by reducing
183 numbers of APCs in the CNS.

184

185 **Blocking CSF-1 depletes inflammatory myeloid APCs in the CNS without affecting quiescent microglia.**

186 We next tested the therapeutic efficacy of anti-CSF-1 MAb treatment. Treatment initiated after onset of
187 disease suppressed clinical EAE (Fig. 3A), and the suppression was maintained up to 45 days after EAE
188 induction, which was the longest period tested (Fig. 3B). Similar to BLZ945, anti-CSF-1 MAb suppressed
189 disease even when treatment was initiated during its more advanced stage (Fig. 3C, D). Mice treated with anti-
190 CSF-1 MAb had fewer $CD45^+$ immune cells in the CNS, including $CD11b^+$, $CD11c^+$, and $CD4^+$ cells (Fig. 3E,
191 F). The treatment decreased frequency of $CD11b^+CD11c^+$ myeloid DCs in the CNS (Supplementarl Fig. 4A),
192 and among $CD11b^+$ myeloid cells, we observed reduced frequencies of $CD11c^+$ microglia, moDCs, cDCs and
193 other $CD11c^+$ cells, indicating that DC populations were preferentially affected (Supplementary Fig. 4B). Anti-
194 CSF-1 treatment reduced the numbers of microglia to those in naïve mice (Fig. 3G), without depleting the
195 entirety of microglia, as was the case with BLZ945. Importantly, the reductions in microglia numbers in anti-
196 CSF-1-treated mice were primarily due to loss of activated inflammatory microglia, which expressed MHC II
197 and/or CD68 (Fig. 3H).

198 We then quantified how anti-CSF-1 treatment affected the composition of myeloid cells in the inflamed
199 CNS (Fig. 3I,J). Anti-CSF-1 treatment reduced the frequencies of moDCs, macrophages, activated microglia and
200 undifferentiated monocytes, but did not affect the frequency of neutrophils. This resulted in a large increase in
201 the frequency of quiescent microglia among $CD11b^+$ cells. Similar to BLZ945-treated mice, anti-CSF-1 treatment
202 resulted in a decrease in MFI for MHC II and CD80, but not CD86 (Fig. 3K), suggesting that inflammatory APCs
203 were preferentially impacted by anti-CSF-1 treatment. Consistent with this, anti-CSF-1-treated mice had a lower
204 frequency of TNF^+MHCII^+ cells in their CNS, including moDCs (Supplemental Fig. 4C,D). An important
205 pathogenic function of moDCs in EAE is production of IL-1β [48]. As expected, a reduced frequency of IL-1β-
206 producing cells was also observed in the CNS of anti-CSF-1 treated EAE mice (Fig. 3L), but, notably, not in
207 BLZ945-treated mice (Supplemental Fig. 3I). Together, these data suggest that blockade of CSF-1 preferentially
208 depletes infiltrating and resident inflammatory myeloid cells, without affecting quiescent microglia.

209

210

211

212 **Anti-CSF1 treatment depletes myeloid cells in white matter lesions, but not microglia in grey matter.**

213 We further tested whether treatment with anti-CSF-1 MAb preferentially depletes inflammatory myeloid
214 cells by examining their distribution in the CNS by microscopy. Anti-CSF-1 MAb treated mice with EAE had
215 reduced white matter demyelination and smaller spinal cord lesions when compared to control mice (Fig. 4A-C).
216 Immunostaining and analysis by confocal microscopy showed that mice treated with control isotype MAb had
217 large numbers of Iba$^+$ cells throughout the spinal cord (Fig. 4D-G). In contrast, mice treated with anti-CSF-1 MAb
218 had notably fewer Iba$^+$ cells and were similar to healthy naïve controls. BLZ945 treatment depleted virtually all
219 Iba$^+$ cells in both white and grey matter. Anti-CSF-1-treated mice also had reduced density of Iba1$^+$ and
220 Iba$^+$CD68$^+$ inflammatory myeloid cells both within regions infiltrated with immune cells and in immediately
221 surrounding areas, but not further into the grey matter (Fig. 4E,F). Treatment with anti-CSF-1 reduced microglial
222 proliferation/activation in the grey matter, reducing numbers of grey matter microglia to levels found in naïve
223 mice (Fig. 4G). Together, these data indicate that anti-CSF-1 treatment primarily targets inflammatory myeloid
224 cells in CNS lesions without depleting quiescent microglia in the grey matter. Further, the depletion of
225 inflammatory myeloid cells in inflamed areas of the white matter precluded alterations to microglia in normally-
226 appearing white and gray matter at sites distant from inflamed areas of the white matter [4, 49-51], indicating an
227 overall reduction in CNS inflammation.

228

229 **CSF-1R inhibition depletes myeloid DCs and monocytes in peripheral lymphoid compartments.**

230 Treatment with BLZ945 delayed onset of disease, whereas anti-CSF-1 treatment did not. This difference
231 could be due to diminished priming of encephalitogenic T cell responses in peripheral lymphoid organs of
232 BLZ945-treated mice, resulting in failure to initiate disease in the CNS. To test this possibility, we treated
233 immunized mice with either BLZ945 or anti-CSF-1 MAb and sacrificed them during the priming phase of EAE,
234 on day 8 p.i. We quantified the immune cells in blood, draining lymph nodes (dLN) and spleen, and found no
235 difference in overall numbers of CD45$^+$ cells in any tissues examined from BLZ945- or anti-CSF-1-treated mice
236 compared to control animals (Supplemental Fig. 5). We did, however, observe a decrease in the numbers of
237 CD11b$^+$ cells in all tissues examined from BLZ945-treated mice, but not from anti-CSF-1-treated mice
238 (Supplemental Fig. 5A-C). We noted a decrease in CD11b$^+$CD11c$^+$ cells in some peripheral lymphoid organs in

239 both BLZ945- and anti-CSF-1-treated mice, including a decrease in moDCs. Notably, numbers of monocytes
240 were reduced in all examined tissues from BLZ945-treated mice, but not from anti-CSF-1-treated mice
241 (Supplemental Fig 6A-F).

242 We tested whether reductions in myeloid DCs in the spleen and dLNs would diminish MOG_{35-55}-specific
243 T cells responses, but did not find reduced proliferation of cells from either BLZ945- or anti-CSF-1-treated
244 animals when compared to control animals (Supplemental Fig. 6G,H). We also measured antigen-specific
245 proliferation at day 16 p.i. and found a reduction in proliferation of splenocytes from BLZ945-treated mice, but
246 not of cells from dLNs. The reduction was likely due to fewer APCs, rather than to intrinsic differences in APC
247 function, as co-culture of equal numbers of $CD11c^+$ cells purified from spleens of vehicle- or BLZ945-treated
248 mice with $CD4^+$ T cells from 2D2 mice elicited similar levels of proliferation (Supplemental Fig. 6I,J). These data
249 show that myeloid DCs are impacted by CSF-1R inhibition, but that this only modestly affects the development
250 of myelin antigen-specific responses. Thus, delayed onset of disease in BLZ945-treated animals is likely due to
251 factors other than impaired development of MOG_{35-55}-specific T cells responses.

252

253 **CSF-1R signaling promotes survival/proliferation of BM-derived moDCs, but not their APC function.**

254 We tested how CSF-1R signaling influences the numbers of DCs by generating BMDCs with GM-CSF
255 and IL-4 [52], and neutralizing CSF-1 and CSF-1R with MAbs. Cultures with either anti-CSF-1 or anti-CSF-1R
256 MAbs contained fewer $CD11c^+MHCII^{Hi}$ DCs (Fig. 5A). This was correlated with a decreased ratio of live/dead
257 cells after LPS treatment (Fig. 5B), suggesting that survival of BMDCs was negatively impacted by the absence
258 of CSF-1R signaling. CSF-1R signaling was not important for development of APC function of BMDCs as there
259 was only a small reduction in the frequency of $CD11c^+MHCII^+$ among live $CD11b^+$ cells (Fig. 5C,D) and co-culture
260 with 2D2 $CD4^+$ T cells revealed no differences in eliciting the proliferation of 2D2 T cells (Fig. 5E). To confirm
261 that these findings are applicable to monocyte-derived BMDCs, we purified $CD11b^+Ly6G^-Ly6C^{Hi}$ monocytes from
262 the BM of $CD45.1^+$ mice, mixed them with total BM cells from $CD45.2^+$ mice, and then blocked CSF-1R signaling
263 during their development into BMDCs. Consistent with total BM cultures, blockade of CSF-1R signaling did not
264 affect the frequency of $CD11c^+MHCII^{Hi}CD45.1^+$ monocyte-derived cells (Fig. 5F,G), but caused a ~75% reduction
265 in their numbers (Fig. 5H). Together, these data indicate that CSF-1R signaling promotes the survival of moDCs,

266 rather than their differentiation and APC function, which is consistent with the role of CSF-1R signaling in
267 maintaining myeloid cell populations [9-11].

268

269 **Blocking CSF-1R signaling or CSF-1 reduces numbers of CCL2- and CCR2-expressing myeloid cells in**
270 **the CNS during EAE.**

271 We observed that numbers of monocytes/moDCs were greatly reduced in the CNS of mice with EAE
272 during CSF-1R inhibition. Given that monocyte recruitment into the CNS via CCL2/CCR2 signaling is essential
273 to EAE pathology [53, 54], and that several reports have shown that CSF-1 induces CCL2 production by
274 monocytes [55-57], we examined CCL2 production in the CNS of BLZ945- and anti-CSF-1-treated mice with
275 EAE. The vast majority of $CCL2^+$ cells were $CD45^+$ (Supplemental Fig. 8A). Among $CD45^+$ cells, there was a
276 reduction in numbers of $CCL2^+$ cells in both BLZ945- and anti-CSF-1-treated animals (Supplemental Fig. 7A, D).
277 The majority of $CCL2^+$ cells were $CD11b^+Ly6C^+$ (Supplemental Fig. 7B,C,E,F), indicating that monocyte-derived
278 cells are a relevant source of CCL2 in the CNS during EAE. Most $CCL2^+$ cells were TNF^+MHC II^+ inflammatory
279 myeloid cells (Supplemental Fig. 8B,C,F,G). Notably, MFI for CCL2 among $CCL2^+$ cells from anti-CSF-1-treated
280 mice, but not from BLZ945-treated mice, was also reduced (Supplemental Fig. 8E). We also examined $CCR2^+$
281 cells from the CNS of BLZ945- and anti-CSF-1-treated mice. As with CCL2-producing cells, there was a reduction
282 in numbers of $CCR2^+$ cells (Supplemental Fig. 7G,J). Most $CCR2^+$ cells were $CD45^{Hi}CD11b^+Ly6C^+$ cells
283 (Supplemental Fig. 7H,I,K,L), indicating that these were the same cells that produce CCL2. Indeed, nearly all
284 $CCL2^+$ cells were $CCR2^+CD11b^+$ cells in anti-CSF-1-treated mice (Supplemental Fig. 8K). Combined with our *in*
285 *vitro* findings, these data suggest that antagonism of CSF-1R signaling inhibits the survival and proliferation of
286 monocytes/moDCs, resulting in fewer CCL2-producing cells, which then reduces the recruitment of $CCR2^+$ cells
287 in the CNS during EAE.

288

289 **Monocytes remaining in the CNS of anti-CSF-1-treated mice have a transcriptional profile consistent with**
290 **a pro-survival phenotype.**

291 Anti-CSF-1 treatments depleted most (>80% depletion) but not all monocytes and monocyte-derived cells
292 in the CNS of mice with EAE (Supplemental Fig. 10A,B). To identify transcriptional changes that could have

293 enabled some monocytes to persist despite diminished CSF-1 signaling, we sequenced their transcriptome after
294 6 days of treatment, a timepoint that correlated well with maximal disease suppression (gating strategy shown
295 in Supplemental Fig. 9A). There were 412 genes differentially expressed between monocytes from anti-CSF-1-
296 and control MAb-treated mice (Supplemental Fig. 10C,D). We utilized the DAVID bioinformatics database [58,
297 59] to identify gene ontology, and KEGG pathway terms that were significantly enriched among the differentially
298 expressed genes. Among GO terms identified as significantly enriched, the largest percentage of genes were
299 involved in cell division (Supplemental Fig. 10E and Supplemental Fig. 9B). Among enriched KEGG pathways
300 in these monocytes, the module with the greatest number of genes was the PI3K-Akt signaling pathway
301 (Supplemental Fig. 10F and Supplemental Fig. 9C), which controls proliferation [60]. Among genes in this
302 pathway, a number of growth factor receptors and transcription factors were upregulated, including *Flt1*
303 (VEGFR), *Myb*, *Kit*, *Pdgfrb*, and *Fgfr1* (Supplemental Fig. 10G). These data suggest that monocytes in the CNS
304 of anti-CSF-1-treated mice survive by upregulation of alternative growth factor receptors, which compensate for
305 diminished CSF-1R signaling.

306

307 **BM-derived immune cells are major contributors to CSF-1R-dependent pathology in EAE.**

308 Inhibition of CSF-1R signaling during EAE, either by direct blocking of CSF-1R kinase activity or by
309 neutralizing CSF-1, diminished numbers of moDCs and microglia, suggesting that disease suppression was due
310 to reduced numbers of one or both of these cell types. To further test the role of CSF-1R signaling in monocytes
311 and microglia in EAE, we developed a genetic model for *Csf1r* deletion that circumvents the perinatal lethality of
312 conventional *Csf1r* knockout mice [61]. We crossed UBC-CreERT2 mice [62] and *Csf1r*$^{fl/fl}$ mice [63] to generate
313 CSF1RiKO mice which have tamoxifen-inducible Cre-mediated deletion of *Csf1r*. Tamoxifen-treated adult
314 CSF1RiKO mice had 70%-100% reduced CSF-1R protein in western blots of cell lysates from the spleen, dLN
315 and CNS (Supplemental Fig. 11A). Next, we treated CSF1RiKO mice with tamoxifen for 5 days and rested them
316 for additional 7-14 days before immunization to induce EAE. CSF1R-iKO mice developed milder EAE than
317 control mice, without a delay in disease onset (Fig. 6A,B, Supplemental Fig. 11B). The tamoxifen pre-treatment
318 led to sustained reduction of CNS moDCs for the duration of observation (~30 days p.i.) (Fig. 6C,D). In contrast,
319 microglia were initially efficiently depleted, but by ~30 days p.i. microglia numbers had recovered to near normal,
320 indicating incomplete knockout of *Csf1r* in microglia progenitors. Nevertheless, microglia were substantially

321 reduced at the time of immunization and until disease peak (~day 20 p.i.). Thus, CSF1RiKO mice enable efficient
322 depletion of CSF-1R in adult mice without the developmental defects present in conventional CSF-1R knockout
323 mice; the depletion of moDCs is long lasting, whereas the depletion of microglia is transient.

324 To determine the relative contributions of CSF-1R signaling in monocytes and microglia to EAE, we
325 generated BM-chimeras by reconstituting treosulfan-conditioned WT and CSF1RiKO recipient mice with either
326 WT or CSF1RiKO BM. We used the BM-conditioning agent treosulfan because it does not cross or affect the
327 BBB, does not induce a cytokine storm, nor does it enable engraftment of peripheral myeloid cells into the CNS,
328 as has been observed in irradiation-induced BM chimeras [64-66]. Pre-conditioning with treosulfan was highly
329 efficient for establishing chimerism, with >90% of peripheral immune cells in chimera mice being of donor BM
330 origin (Supplemental Fig. 11C). Following 8 weeks of BM-reconstitution, mice were treated with tamoxifen to
331 knockout *Csf1r* and then immunized to induce EAE (Fig. 6E). Both WT and CSF1R-iKO mice reconstituted with
332 WT BM developed typical EAE, whereas WT mice reconstituted with CSF1RiKO BM developed attenuated EAE,
333 similar to CSF1RiKO mice reconstituted with CSF1RiKO BM. These data show that BM-derived cells are a major
334 contributor to CSF-1R-dependent pathology during EAE, whereas microglia play a less important role.

335 Lastly, we sought to understand the role of CSF-1R in survival of monocytes during EAE. We utilized
336 mixed-BM chimeras generated by reconstitution of WT mice with WT and CSF1R-iKO BMs (1:1). 50% WT BM
337 is sufficient to drive the development of typical EAE [6, 67]. Indeed, mice reconstituted with a mixture of WT and
338 CSF1R-iKO BMs and pre-treated with tamoxifen developed EAE equivalent to mice reconstituted with WT BM
339 (Fig. 6F). In the CNS, we found a lower frequency of CSF1R-iKO monocyte-derived cells when compared to WT
340 cells (Fig. 6G, Supplemental Fig. 11D). These data suggest that CSF-1R signaling maintains monocytic cells in
341 the CNS during EAE.

342

343 **DISCUSSION**

344 We show that blocking CSF-1R, CSF-1 and IL-34 has differential effects on EAE. Overall, blocking either CSF-
345 1R or CSF-1 resulted in suppression of clinical disease and diminished CNS inflammation and demyelination.
346 Notably, blocking CSF-1R and CSF-1 produced distinct effects on the composition of immune cells in the CNS
347 during EAE. Numbers of microglia and monocyte-derived cells were the most reduced by CSF-1R inhibition.

348 Treatment with BLZ945 depleted virtually all microglia, whereas anti-CSF-1 treatment preferentially depleted
349 inflammatory microglia, reducing their number to similar numbers as in naïve mice. Moreover, depletion of
350 myeloid cells in anti-CSF-1-treated mice was limited to CNS lesions and adjacent areas, while grey matter
351 microglia had a similar appearance as naïve mice. The notably lower microglia depletion by anti-CSF-1 MAb
352 than with BLZ945 did not result in less effective disease suppression, but rather improved long-term therapeutic
353 efficacy when compared to BLZ945 treatments, suggesting that full therapeutic benefit can be achieved without
354 applying a maximally ablative approach. Limited depletion of microglia by anti-CSF-1 MAb may therefore be
355 advantageous in MS therapy, as it carries fewer potential risks than widespread microglia depletion likely would.
356 Favoring a milder approach for depletion of myeloid cells is supported by a finding that PLX5622, a commonly
357 used inhibitor of CSF-1R kinase activity, in addition to depleting microglia, also causes long-term and widespread
358 systemic changes to myeloid and lymphoid compartments [68]. It is likely that other small molecule inhibitors of
359 CSF-1R, including BLZ945, induce similar changes, but it is also likely that blocking CSF-1 induces fewer
360 systemic changes because of compensatory IL-34 signaling and more restricted tissue distribution of the MAb
361 compared to small molecule inhibitors, as exemplified by our findings in the CNS. For example, other organs
362 with blood barriers, such as testes, eye, and thymus, all of which express CSF-1R [69], would likely be less
363 affected by anti-CSF-1 MAb than a small molecule inhibitor, which could more readily penetrate the barriers and
364 inhibit both CSF-1 and IL-34 signaling.

365 The limited microglia depletion by anti-CSF-1 MAb is likely due to the presence of IL-34 in non-inflamed
366 CNS areas, where it maintains homeostatic microglia survival. Indeed, it has been shown that systemic injections
367 of anti-CSF-1 MAb do not deplete microglia [70]. This is consistent with studies showing that IL-34 accounts for
368 approximately 70% of CSF-1R signaling in healthy brain [23], and that anti-CSF-1 MAb is unlikely to penetrate
369 into the normal CNS parenchyma, as only a miniscule fraction of Abs crosses the intact BBB [10, 30]. Thus, it is
370 expected that neutralization of CSF-1 in the CNS occurs primarily in active lesions, where BBB is leaky, resulting
371 in localized depletion of inflammatory myeloid cells. This model is analogous to the role of CSF-1R ligands in the
372 skin, where IL-34 maintains Langerhans cells in steady state. However, during skin inflammation, IL-34 becomes
373 dispensable, as infiltrated immune cells produce CSF-1 and maintain/expand numbers of Langerhans cells [45].
374 It should be noted, though, that CSF-1R signaling is not in itself inherently pro-inflammatory by eliciting
375 inflammatory phenotype in myeloid cells, but can have such a net effect by simply maintaining their survival

376 during inflammation. In fact, in the absence of inflammation, CSF-1R signaling induces an
377 immunosuppressive/homeostatic M2 phenotype in macrophages and a resting/quiescent phenotype in microglia
378 [1, 12-26]. Hence, our observations on blockade of CSF-1R signaling in EAE are the net effect of abrogating
379 both pro- and anti-inflammatory functions of CSF-1R signaling, with the pro-inflammatory ones predominating.
380 Together, our findings suggest that CSF-1 promotes inflammation in EAE by expansion of microglia and
381 monocyte-derived myeloid cells, whereas IL-34 maintains microglia in non-inflamed CNS areas, similar to the
382 healthy CNS.

383 Our data suggest that IL-34 does not play a significant role in EAE pathology. This can be explained by
384 notably more widespread and abundant expression of CSF-1 compared with IL-34 [71]. It is likely that in most
385 cases CSF-1 can therefore compensate for lack of IL-34. This interpretation is supported by a study that has
386 demonstrated that CSF-1 in inflamed sites becomes the dominant CSF-1R ligand, even in tissue (skin) where
387 IL-34, but not CSF-1, is expressed in steady state [45]. Thus, although our data suggest that blockade of IL-34
388 with MAb may have been incomplete due to the development of anti-rat IgG responses, it is probable that
389 abundantly produced CSF-1 in CNS lesions mediates most CSF-1R signaling, and that blockade of IL-34
390 therefore does not have an effect on EAE.

391 Our in vitro studies with BMDCs show that the primary effect of CSF-1R inhibition is limiting the number
392 of myeloid DCs in these cultures rather than affecting their APC functions. These data are consistent with a body
393 of literature showing that CSF-1R signaling in myeloid cells chiefly provides proliferative and anti-apoptotic
394 signals for maintenance of the population size [34]. This concept is exemplified by differences between animals
395 lacking CSF-1 and IL-34, in which CSF-1 knockout mice have reduced numbers of osteoclasts and monocytes
396 but only a modest reduction in microglia [32]. In contrast, IL-34 knockout mice have greatly reduced numbers of
397 microglia and Langerhans cells, but largely normal numbers of other tissue resident macrophages [32]. Thus,
398 CSF-1R inhibition is likely to suppress inflammation in EAE by reducing the population size of inflammatory
399 myeloid cells in the CNS.

400 Transcriptional profiling of monocytes that remained in the CNS after anti-CSF-1 treatment suggests that
401 they avoid death via upregulation of growth factor receptors known to promote myeloid cell survival, including
402 Kit [72-74]. Notably, upregulation of these genes has been reported in myeloid cell cancers [75-79]. However, a
403 number of questions regarding these surviving monocytes remain, such as: are they a normally present

404 subpopulation among CNS monocytes, or were they induced by neutralization of CSF-1; do they eventually
405 succumb to early death compared to monocytes that have been receiving CSF-1R signaling; do all monocytes
406 lacking CSF-1R signaling acquire this phenotype before death; and, what is the capacity of the surviving
407 monocytes to perpetuate inflammation? It is possible that altered phenotype of surviving monocytes is less pro-
408 inflammatory because of diminished effector functions, such as cytokine and chemokine production.

409 Our in vivo studies indicate an additional mechanism of EAE suppression by inhibition of CSF-1R
410 signaling, namely, reduced recruitment of immune cells to the CNS. We found reduction in numbers of both
411 CCL2- and CCR2-expressing cells when mice were treated with BLZ945 or anti-CSF-1 MAb. Most cells that
412 expressed CCL2 and CCR2 were monocytes/moDCs, which suggests a model whereby monocytes that infiltrate
413 the CNS produce CCL2, thus amplifying inflammation by further recruitment of CCR2-expressing cells. Given
414 that CSF-1R signaling in monocytes/macrophages induces CCL2 expression [55-57], this suggests that its
415 blockade reduces CNS inflammation by two mechanisms: 1) by reducing numbers of cells that produce CCL2,
416 and 2) by reducing CCL2 production of surviving cells, which together amounts to greatly diminished CCL2 levels
417 in the CNS during EAE. This is consistent with an essential role of CCL2 and CCR2 in EAE, since interventions
418 that affect them attenuate disease [80-82]. It is also possible that in addition to monocytes, reduction in CCL2
419 directly affects recruitment of pathogenic $CCR2^+$ Th cells to the CNS, given a report that CCR2 drives their
420 recruitment to the CNS [80]. Taken together with our result showing reduced GM-CSF and IL-1β production in
421 the CNS, it is likely that CSF-1R inhibition suppresses EAE by depleting CCL2- and IL-1β-expressing APCs. IL-
422 1β has an essential role in EAE [6, 48, 83, 84] by acting on $CD4^+$ T cells to promote their proliferation and GM-
423 CSF production; GM-CSF is also essential to EAE development by acting on monocytes to induce their pro-
424 inflammatory phenotype and IL-1β production, thus completing a positive feedback loop that sustains
425 inflammation [85]. Inhibition of CSF-1R signaling likely interrupts this pro-inflammatory feedback loop, resulting
426 in EAE suppression.

427 To determine the relative contributions of CSF-1R signaling in monocytes and microglia to EAE, we
428 developed CSF1R-iKO mice. Our BM chimera experiments indicate that a lack of CSF-1R signaling in BM-
429 derived cells, rather than in CNS-resident cells (e.g. microglia), is responsible for the EAE suppression. However,
430 the transient nature of microglia depletion in CSF-1RiKO mice prevents us from concluding that microglia are
431 entirely dispensable for EAE development. Our experiments with mixed BM chimeras support the view that CSF-

432 1R functions as a growth factor receptor for monocytes and their progeny [9-11]. However, it is worth noting that
433 treating WT mice with BLZ945 induced more profound reduction in CNS moDCs than in mixed BM chimeras.
434 This may be explained by the presence of WT monocytes in mixed BM-chimeras, which are able to produce
435 CCL2, and therefore maintain recruitment of monocytes into the CNS. This is consistent with a model in which
436 CSF-1R signaling maintains numbers of monocytes and cells that differentiate from them, by promoting their
437 survival/proliferation, but also by potentiating their recruitment into the CNS via CCL2 production, which are both
438 reported functions of CSF-1R [9-11, 55-57].

439 Therapies using anti-CSF-1 MAb and small molecule inhibitors of CSF-1R have been tested in multiple
440 clinical trials for autoimmune and oncological diseases [86-91]. These trials have demonstrated that blockade of
441 CSF-1/CSF-1R is well tolerated by patients [90, 92, 93]. Targeting CSF-1/CSF-1R in MS has not been tested,
442 but agents used in trials for other diseases would likely be suitable for testing in MS. Moreover, because CSF-
443 1R signaling is not required by myeloid progenitors residing in the BM or CNS (for microglia) [34, 94], the effects
444 of these treatments would be largely reversible. Indeed, there is complete repopulation of microglia within one
445 week after cessation of treatment with CSF-1R inhibitors [94]. A treatment modality can be envisioned whereby
446 blocking CSF-1R signaling for therapy of MS would follow an intermittent regimen, given for a period of time,
447 instead of continuously. Thus, as a potential therapy for MS, targeting CSF-1/CSF-1R offers several advantages,
448 including the potential of being readily translatable to clinical testing with already existing therapeutic agents.

449 In conclusion, blocking CSF-1R signaling ameliorates EAE by depleting inflammatory APCs in the CNS.
450 MS therapy with anti-CSF-1 MAb could be a preferred approach, because, unlike small molecule inhibitors of
451 CSF-1R, it preserves quiescent microglia and their homeostatic functions, as well as other IL-34 functions, such
452 as maintenance of Langerhans cells. Limited depletion of microglia by anti-CSF-1 treatment, however, does not
453 diminish its therapeutic effect compared to BLZ945 treatment. Reducing CSF-1R signaling via neutralization of
454 CSF-1 could therefore be a novel strategy for therapy of MS.

455

456

457

458

459 **MATERIALS AND METHODS**

460 *More information is available in supplemental materials.*

461 **Mice**

462 All mice used in this study were on C57BL/6J genetic background. Mice were either obtained from The Jackson
463 Laboratories (Bar Harbor, Maine) or bred in-house. All experimental procedures were approved by the
464 Institutional Animal Care and Use Committee of Thomas Jefferson University. CSF1RiKO mice were generated
465 by breeding UBC-CreERT2 (The Jackson Laboratories, Stock #007001) with $Csf1r^{flox}$ mice (The Jackson
466 Laboratories, Stock #021212). Genotyping was performed as recommended by The Jackson Laboratories.
467 CD45.1 mice (B6.SJL-Ptprca Pepcb/BoyJ, Stock #002014) were obtained from The Jackson Laboratories.

468

469 **Induction and Scoring of EAE**

470 EAE was induced by immunization with 1:1 emulsion of PBS and complete Freund's adjuvant (CFA) containing
471 5 mg/mL heat killed *M. tuberculosis* (BD Biosciences) and 1 mg/mL MOG_{35-55} peptide (Genscript). Mice were
472 immunized on both flanks by subcutaneous injection of the emulsion for a total of 200 µL. Pertussis toxin was
473 i.p. injected on days 0 and 2 post-immunization at 200 ng per dose. Mice were scored according to the following
474 scale: 0 - No clinical symptoms. 0.5 - Partial paralysis of the tail or waddling gait. 1.0 - Full paralysis of the tail.
475 1.5 - Full paralysis of the tail and waddling gait. 2.0 - Partial paralysis in one leg. 2.5 - Partial paralysis in both
476 legs or one leg paralyzed. 3.0 - Both legs paralyzed. 3.5 - Ascending paralysis. 4.0 - Paralysis above the hips.
477 4.5 – Moribund; mouse being unable to right itself for 30 seconds. 5.0 - Death.

478

479 **BLZ945 Preparation and Treatment**

480 BLZ945 (Selleck Chemicals and MedChemExpress) was prepared from powder in 20% captisol at 12 mg/mL.
481 Mice were treated with BLZ945 by oral gavage with 4-6 mg/treatment/day. In initial experiments, we used BLZ945
482 prepared in 20% captisol, and 20% captisol as control, which were a generous gift from Novartis International
483 AG.

484

485 ***In vivo* CSF-1, Anti-CSF-1, Anti-IL-34, and Anti-CSF-1R Treatments**

486 Recombinant CSF-1 (4 µg/dose; R&D Systems) was given to EAE mice on days 4, 8, 12, 16 post immunization
487 (p.i.) by intraperitoneal (i.p.) injection. All MAb treatments were also given by i.p. injection. Prophylactic
488 treatments with anti-CSF-1 (200 µg/dose; clone: 5A1; Bio X Cell) started on day 0 p.i. and were given every
489 other day until disease onset, when dosing was changed to every day. In therapeutic treatments, MAb was given
490 every day, starting on days indicated in figures, for the duration of acute phase of the disease (typically days 11-
491 25 p.i.), then switched to every other day for the rest of the experiments. Equal amounts of control IgG1 (Clone:
492 HPRN; Bio X Cell) were used to treat control mice. Mice were treated with anti-IL-34 MAb (100 µg/dose; Clone:
493 780310; Novus Biologicals) every other day for the duration of the experiment. Anti-CSF-1R Mab (400 µg/dose;
494 Clone: AFS98; Bio X Cell) was given every other day. In experiments with anti-IL-34 and anti-CSF-1R MAbs,
495 equal amounts of control IgG2A (Clone: 2A3; Bio X Cell) were given to control mice.

496

497

498

499

500

501

502

503

504

505

506

507

508 **Author Contributions**

509 Bogoljub Ciric and Daniel Hwang were responsible for the conceptualization of this project. Daniel Hwang was
510 responsible for carrying out experiments and analysis of data.

511 Larissa Lumi Watanabe Ishikawa, Alexandra Boehm, Ziver Sahin, Giacomo Casella, Soohwa Jang, and
512 Maryamsadat Seyedsadr assisted in carrying out experiments.

513 Michael Gonzalez, James Garifallo and Hakon Hakonarson were responsible for RNA sequencing experiments
514 and assisted with analysis of RNA sequencing data.

515 Guang-Xian Zhang, Weifeng Zhang, Dan Xiao, and Abdolmohamad Rostami assisted with manuscript
516 preparation and provided helpful insights in interpreting data.

517

518 **Acknowledgments**

519 We thank Katherine Regan for editing the manuscript. We thank Medac Germany for the kind gift of treosulfan
520 for our BM chimera studies.

521

522 **Funding**

523 This work was supported by a grant from the National Multiple Sclerosis Society (RG-1803-30491) to B. Ciric.

524

525

526

527

528

529

530

531 **REFERENCES**

532 1. Pyonteck, S.M., et al., *CSF-1R inhibition alters macrophage polarization and blocks glioma progression.* Nat Med,
533 2013. **19**(10): p. 1264-72. PMC3840724 PMID: 24056773.
534 2. Lassmann, H. and M. Bradl, *Multiple sclerosis: experimental models and reality.* Acta Neuropathol, 2017. **133**(2):
535 p. 223-244. PMC5250666 PMID: 27766432.
536 3. Ramaglia, V., et al., *Multiplexed imaging of immune cells in staged multiple sclerosis lesions by mass cytometry.*
537 Elife, 2019. **8**. PMC6707785 PMID: 31368890.
538 4. Zrzavy, T., et al., *Loss of 'homeostatic' microglia and patterns of their activation in active multiple sclerosis.* Brain,
539 2017. **140**(7): p. 1900-1913. PMC6057548 PMID: 28541408.
540 5. Machado-Santos, J., et al., *The compartmentalized inflammatory response in the multiple sclerosis brain is*
541 *composed of tissue-resident CD8+ T lymphocytes and B cells.* Brain, 2018. **141**(7): p. 2066-2082. PMC6022681
542 PMID: 29873694.
543 6. Croxford, A.L., et al., *The Cytokine GM-CSF Drives the Inflammatory Signature of CCR2+ Monocytes and Licenses*
544 *Autoimmunity.* Immunity, 2015. **43**(3): p. 502-14. PMID: 26341401.
545 7. Fife, B.T., et al., *CC chemokine receptor 2 is critical for induction of experimental autoimmune encephalomyelitis.*
546 J Exp Med, 2000. **192**(6): p. 899-905. PMC2193286 PMID: 10993920.
547 8. Giles, D.A., et al., *CNS-resident classical DCs play a critical role in CNS autoimmune disease.* J Clin Invest, 2018.
548 **128**(12): p. 5322-5334. PMC6264723 PMID: 30226829.
549 9. Percin, G.I., et al., *CSF1R regulates the dendritic cell pool size in adult mice via embryo-derived tissue-resident*
550 *macrophages.* Nat Commun, 2018. **9**(1): p. 5279. PMC6290072 PMID: 30538245.
551 10. Hume, D.A. and K.P. MacDonald, *Therapeutic applications of macrophage colony-stimulating factor-1 (CSF-1)*
552 *and antagonists of CSF-1 receptor (CSF-1R) signaling.* Blood, 2012. **119**(8): p. 1810-20. PMID: 22186992.
553 11. MacDonald, K.P., et al., *The colony-stimulating factor 1 receptor is expressed on dendritic cells during*
554 *differentiation and regulates their expansion.* J Immunol, 2005. **175**(3): p. 1399-405. PMID: 16034075.
555 12. Fleetwood, A.J., et al., *Granulocyte-macrophage colony-stimulating factor (CSF) and macrophage CSF-dependent*
556 *macrophage phenotypes display differences in cytokine profiles and transcription factor activities: implications*
557 *for CSF blockade in inflammation.* J Immunol, 2007. **178**(8): p. 5245-52. PMID: 17404308.
558 13. Sierra-Filardi, E., et al., *Activin A skews macrophage polarization by promoting a proinflammatory phenotype and*
559 *inhibiting the acquisition of anti-inflammatory macrophage markers.* Blood, 2011. **117**(19): p. 5092-101. PMID:
560 21389328.
561 14. Verreck, F.A., et al., *Human IL-23-producing type 1 macrophages promote but IL-10-producing type 2*
562 *macrophages subvert immunity to (myco)bacteria.* Proc Natl Acad Sci U S A, 2004. **101**(13): p. 4560-5.
563 PMC384786 PMID: 15070757.
564 15. Hamilton, J.A., *Colony-stimulating factors in inflammation and autoimmunity.* Nat Rev Immunol, 2008. **8**(7): p.
565 533-44. PMID: 18551128.
566 16. Komohara, Y., et al., *Possible involvement of the M2 anti-inflammatory macrophage phenotype in growth of*
567 *human gliomas.* J Pathol, 2008. **216**(1): p. 15-24. PMID: 18553315.
568 17. Foucher, E.D., et al., *IL-34 induces the differentiation of human monocytes into immunosuppressive*
569 *macrophages. antagonistic effects of GM-CSF and IFNgamma.* PLoS One, 2013. **8**(2): p. e56045. PMC3568045
570 PMID: 23409120.
571 18. Smith, A.M., et al., *M-CSF increases proliferation and phagocytosis while modulating receptor and transcription*
572 *factor expression in adult human microglia.* J Neuroinflammation, 2013. **10**: p. 85. PMC3729740 PMID:
573 23866312.
574 19. Guan, Y., et al., *Antigen presenting cells treated in vitro by macrophage colony-stimulating factor and*
575 *autoantigen protect mice from autoimmunity.* J Neuroimmunol, 2007. **192**(1-2): p. 68-78. PMC2743086 PMID:
576 18006080.
577 20. MacDonald, K.P., et al., *An antibody against the colony-stimulating factor 1 receptor depletes the resident subset*
578 *of monocytes and tissue- and tumor-associated macrophages but does not inhibit inflammation.* Blood, 2010.
579 **116**(19): p. 3955-63. PMID: 20682855.
580 21. Hamilton, J.A. and A. Achuthan, *Colony stimulating factors and myeloid cell biology in health and disease.* Trends
581 Immunol, 2013. **34**(2): p. 81-9. PMID: 23000011.

582 22. Djelloul, M., et al., *RAE-1 expression is induced during experimental autoimmune encephalomyelitis and is*
583 *correlated with microglia cell proliferation.* Brain Behav Immun, 2016. **58**: p. 209-217. PMID: 27444966.
584 23. Chitu, V., et al., *Emerging Roles for CSF-1 Receptor and its Ligands in the Nervous System.* Trends Neurosci, 2016.
585 **39**(6): p. 378-393. PMC4884457 PMID: 27083478.
586 24. Smith, A.M., et al., *Adult human glia, pericytes and meningeal fibroblasts respond similarly to IFNy but not to*
587 *TGFbeta1 or M-CSF.* PLoS One, 2013. **8**(12): p. e80463. PMC3855168 PMID: 24339874.
588 25. Caescu, C.I., et al., *Colony stimulating factor-1 receptor signaling networks inhibit mouse macrophage*
589 *inflammatory responses by induction of microRNA-21.* Blood, 2015. **125**(8): p. e1-13. PMC4335087 PMID:
590 25573988.
591 26. De, I., et al., *CSF1 overexpression has pleiotropic effects on microglia in vivo.* Glia, 2014. **62**(12): p. 1955-67.
592 PMC4205273 PMID: 25042473.
593 27. Hagan, N., et al., *CSF1R signaling is a regulator of pathogenesis in progressive MS.* Cell Death Dis, 2020. **11**(10):
594 p. 904. PMC7584629 PMID: 33097690.
595 28. Crespo, O., et al., *Tyrosine kinase inhibitors ameliorate autoimmune encephalomyelitis in a mouse model of*
596 *multiple sclerosis.* J Clin Immunol, 2011. **31**(6): p. 1010-20. PMC3225802 PMID: 21847523.
597 29. Nissen, J.C., et al., *Csf1R inhibition attenuates experimental autoimmune encephalomyelitis and promotes*
598 *recovery.* Exp Neurol, 2018. **307**: p. 24-36. PMID: 29803827.
599 30. Freskgard, P.O. and E. Urich, *Antibody therapies in CNS diseases.* Neuropharmacology, 2017. **120**: p. 38-55.
600 PMID: 26972827.
601 31. Denny, W.A. and J.U. Flanagan, *Small-molecule CSF1R kinase inhibitors; review of patents 2015-present.* Expert
602 Opin Ther Pat, 2021. **31**(2): p. 107-117. PMID: 33108917.
603 32. Wang, Y. and M. Colonna, *Interkeukin-34, a cytokine crucial for the differentiation and maintenance of tissue*
604 *resident macrophages and Langerhans cells.* Eur J Immunol, 2014. **44**(6): p. 1575-81. PMC4137395 PMID:
605 24737461.
606 33. Boulakirba, S., et al., *IL-34 and CSF-1 display an equivalent macrophage differentiation ability but a different*
607 *polarization potential.* Sci Rep, 2018. **8**(1): p. 256. PMC5762882 PMID: 29321503.
608 34. Stanley, E.R. and V. Chitu, *CSF-1 receptor signaling in myeloid cells.* Cold Spring Harb Perspect Biol, 2014. **6**(6).
609 PMC4031967 PMID: 24890514.
610 35. Nakamichi, Y., N. Udagawa, and N. Takahashi, *IL-34 and CSF-1: similarities and differences.* J Bone Miner Metab,
611 2013. **31**(5): p. 486-95. PMID: 23740288.
612 36. Nandi, S., et al., *Receptor-type protein-tyrosine phosphatase zeta is a functional receptor for interleukin-34.* J Biol
613 Chem, 2013. **288**(30): p. 21972-86. PMC3724651 PMID: 23744080.
614 37. Kuboyama, K., et al., *Inactivation of Protein Tyrosine Phosphatase Receptor Type Z by Pleiotrophin Promotes*
615 *Remyelination through Activation of Differentiation of Oligodendrocyte Precursor Cells.* J Neurosci, 2015. **35**(35):
616 p. 12162-71. PMC6605312 PMID: 26338327.
617 38. Sarahrudi, K., et al., *Elevated levels of macrophage colony-stimulating factor in human fracture healing.* J Orthop
618 Res, 2010. **28**(5): p. 671-6. PMID: 19950360.
619 39. Aharinejad, S., et al., *Elevated CSF1 serum concentration predicts poor overall survival in women with early*
620 *breast cancer.* Endocr Relat Cancer, 2013. **20**(6): p. 777-83. PMID: 24016870.
621 40. Kawano, Y., et al., *Measurement of serum levels of macrophage colony-stimulating factor (M-CSF) in patients*
622 *with uremia.* Exp Hematol, 1993. **21**(2): p. 220-3. PMID: 8425560.
623 41. Moon, S.J., et al., *Increased levels of interleukin 34 in serum and synovial fluid are associated with rheumatoid*
624 *factor and anticyclic citrullinated peptide antibody titers in patients with rheumatoid arthritis.* J Rheumatol,
625 2013. **40**(11): p. 1842-9. PMID: 23996288.
626 42. Chang, E.J., et al., *IL-34 is associated with obesity, chronic inflammation, and insulin resistance.* J Clin Endocrinol
627 Metab, 2014. **99**(7): p. E1263-71. PMID: 24712570.
628 43. Wang, H., J. Cao, and X. Lai, *Serum Interleukin-34 Levels Are Elevated in Patients with Systemic Lupus*
629 *Erythematosus.* Molecules, 2016. **22**(1). PMID: 28036035.
630 44. Luo, J., et al., *Colony-stimulating factor 1 receptor (CSF1R) signaling in injured neurons facilitates protection and*
631 *survival.* J Exp Med, 2013. **210**(1): p. 157-72. PMC3549715 PMID: 23296467.
632 45. Wang, Y., et al., *Nonredundant roles of keratinocyte-derived IL-34 and neutrophil-derived CSF1 in Langerhans cell*
633 *renewal in the steady state and during inflammation.* Eur J Immunol, 2016. **46**(3): p. 552-9. PMC5658206 PMID:
634 26634935.

46. Okubo, M., et al., *Macrophage-Colony Stimulating Factor Derived from Injured Primary Afferent Induces Proliferation of Spinal Microglia and Neuropathic Pain in Rats.* PLoS One, 2016. **11**(4): p. e0153375. PMC4829214 PMID: 27071004.
47. Hawley, C.A., et al., *Csf1r-mApple Transgene Expression and Ligand Binding In Vivo Reveal Dynamics of CSF1R Expression within the Mononuclear Phagocyte System.* J Immunol, 2018. **200**(6): p. 2209-2223. PMC5834790 PMID: 29440354.
48. Lin, C.C. and B.T. Edelson, *New Insights into the Role of IL-1beta in Experimental Autoimmune Encephalomyelitis and Multiple Sclerosis.* J Immunol, 2017. **198**(12): p. 4553-4560. PMC5509030 PMID: 28583987.
49. Kim, R.Y., et al., *Astrocyte CCL2 sustains immune cell infiltration in chronic experimental autoimmune encephalomyelitis.* J Neuroimmunol, 2014. **274**(1-2): p. 53-61. PMC4343306 PMID: 25005117.
50. Gushchina, S., et al., *Increased expression of colony-stimulating factor-1 in mouse spinal cord with experimental autoimmune encephalomyelitis correlates with microglial activation and neuronal loss.* Glia, 2018. **66**(10): p. 2108-2125. PMID: 30144320.
51. Nowacki, P., D. Koziarska, and M. Masztalewicz, *Microglia and astroglia proliferation within the normal appearing white matter in histologically active and inactive multiple sclerosis.* Folia Neuropathol, 2019. **57**(3): p. 249-257. PMID: 31588711.
52. Lutz, M.B., et al., *GM-CSF Monocyte-Derived Cells and Langerhans Cells As Part of the Dendritic Cell Family.* Front Immunol, 2017. **8**: p. 1388. PMC5660299 PMID: 29109731.
53. Mildner, A., et al., *CCR2+Ly-6Chi monocytes are crucial for the effector phase of autoimmunity in the central nervous system.* Brain, 2009. **132**(Pt 9): p. 2487-500. PMID: 19531531.
54. Mahad, D., et al., *Modulating CCR2 and CCL2 at the blood-brain barrier: relevance for multiple sclerosis pathogenesis.* Brain, 2006. **129**(Pt 1): p. 212-23. PMID: 16230319.
55. Sierra-Filardi, E., et al., *CCL2 shapes macrophage polarization by GM-CSF and M-CSF: identification of CCL2/CCR2-dependent gene expression profile.* J Immunol, 2014. **192**(8): p. 3858-67. PMID: 24639350.
56. Stutchfield, B.M., et al., *CSF1 Restores Innate Immunity After Liver Injury in Mice and Serum Levels Indicate Outcomes of Patients With Acute Liver Failure.* Gastroenterology, 2015. **149**(7): p. 1896-1909 e14. PMC4672154 PMID: 26344055.
57. Tagliani, E., et al., *Coordinate regulation of tissue macrophage and dendritic cell population dynamics by CSF-1.* J Exp Med, 2011. **208**(9): p. 1901-16. PMC3171096 PMID: 21825019.
58. Huang da, W., B.T. Sherman, and R.A. Lempicki, *Systematic and integrative analysis of large gene lists using DAVID bioinformatics resources.* Nat Protoc, 2009. **4**(1): p. 44-57. PMID: 19131956.
59. Huang da, W., B.T. Sherman, and R.A. Lempicki, *Bioinformatics enrichment tools: paths toward the comprehensive functional analysis of large gene lists.* Nucleic Acids Res, 2009. **37**(1): p. 1-13. PMC2615629 PMID: 19033363.
60. Hemmings, B.A. and D.F. Restuccia, *PI3K-PKB/Akt pathway.* Cold Spring Harb Perspect Biol, 2012. **4**(9): p. a011189. PMC3428770 PMID: 22952397.
61. Chitu, V. and E.R. Stanley, *Regulation of Embryonic and Postnatal Development by the CSF-1 Receptor.* Curr Top Dev Biol, 2017. **123**: p. 229-275. PMC5479137 PMID: 28236968.
62. Ruzankina, Y., et al., *Deletion of the developmentally essential gene ATR in adult mice leads to age-related phenotypes and stem cell loss.* Cell Stem Cell, 2007. **1**(1): p. 113-26. PMC2920603 PMID: 18371340.
63. Li, J., et al., *Conditional deletion of the colony stimulating factor-1 receptor (c-fms proto-oncogene) in mice.* Genesis, 2006. **44**(7): p. 328-35. PMID: 16823860.
64. Capotondo, A., et al., *Brain conditioning is instrumental for successful microglia reconstitution following hematopoietic stem cell transplantation.* Proc Natl Acad Sci U S A, 2012. **109**(37): p. 15018-23. PMC3443128 PMID: 22923692.
65. Goldmann, T., et al., *Origin, fate and dynamics of macrophages at central nervous system interfaces.* Nat Immunol, 2016. **17**(7): p. 797-805. PMC4968048 PMID: 27135602.
66. Kierdorf, K., et al., *Bone marrow cell recruitment to the brain in the absence of irradiation or parabiosis bias.* PLoS One, 2013. **8**(3): p. e58544. PMC3592806 PMID: 23526995.
67. Greter, M., et al., *GM-CSF controls nonlymphoid tissue dendritic cell homeostasis but is dispensable for the differentiation of inflammatory dendritic cells.* Immunity, 2012. **36**(6): p. 1031-46. PMC3498051 PMID: 22749353.

68. Lei, F., et al., *CSF1R inhibition by a small-molecule inhibitor is not microglia specific; affecting hematopoiesis and the function of macrophages.* Proc Natl Acad Sci U S A, 2020. **117**(38): p. 23336-23338. PMC7519218 PMID: 32900927.
69. Sasmono, R.T., et al., *A macrophage colony-stimulating factor receptor-green fluorescent protein transgene is expressed throughout the mononuclear phagocyte system of the mouse.* Blood, 2003. **101**(3): p. 1155-63. PMID: 12393599.
70. Rietkotter, E., et al., *Anti-CSF-1 treatment is effective to prevent carcinoma invasion induced by monocyte-derived cells but scarcely by microglia.* Oncotarget, 2015. **6**(17): p. 15482-93. PMC4558165 PMID: 26098772.
71. Wei, S., et al., *Functional overlap but differential expression of CSF-1 and IL-34 in their CSF-1 receptor-mediated regulation of myeloid cells.* J Leukoc Biol, 2010. **88**(3): p. 495-505. 2924605 PMID: 20504948.
72. Brizzi, M.F., et al., *Regulation of c-kit expression in human myeloid cells.* Stem Cells, 1993. **11 Suppl 2**: p. 42-8. PMID: 7691327.
73. Kusmartsev, S. and D.I. Gabrilovich, *Effect of tumor-derived cytokines and growth factors on differentiation and immune suppressive features of myeloid cells in cancer.* Cancer Metastasis Rev, 2006. **25**(3): p. 323-31. PMC1693571 PMID: 16983515.
74. Berardi, A.C., et al., *Basic fibroblast growth factor mediates its effects on committed myeloid progenitors by direct action and has no effect on hematopoietic stem cells.* Blood, 1995. **86**(6): p. 2123-9. PMID: 7662960.
75. Heo, S.K., et al., *Targeting c-KIT (CD117) by dasatinib and radotinib promotes acute myeloid leukemia cell death.* Sci Rep, 2017. **7**(1): p. 15278. PMC5681687 PMID: 29127384.
76. Qin, H., et al., *FGFR1OP2-FGFR1 induced myeloid leukemia and T-cell lymphoma in a mouse model.* Haematologica, 2016. **101**(3): p. e91-4. PMC4815735 PMID: 26589915.
77. Zhao, L., P. Ye, and T.J. Gonda, *The MYB proto-oncogene suppresses monocytic differentiation of acute myeloid leukemia cells via transcriptional activation of its target gene GFI1.* Oncogene, 2014. **33**(35): p. 4442-9. PMID: 24121275.
78. Demoulin, J.B. and C.P. Montano-Almendras, *Platelet-derived growth factors and their receptors in normal and malignant hematopoiesis.* Am J Blood Res, 2012. **2**(1): p. 44-56. PMC3301440 PMID: 22432087.
79. Song, G., Y. Li, and G. Jiang, *Role of VEGF/VEGFR in the pathogenesis of leukemias and as treatment targets (Review).* Oncol Rep, 2012. **28**(6): p. 1935-44. PMID: 22993103.
80. Kara, E.E., et al., *CCR2 defines in vivo development and homing of IL-23-driven GM-CSF-producing Th17 cells.* Nat Commun, 2015. **6**: p. 8644. PMC4639903 PMID: 26511769.
81. Huang, D.R., et al., *Absence of monocyte chemoattractant protein 1 in mice leads to decreased local macrophage recruitment and antigen-specific T helper cell type 1 immune response in experimental autoimmune encephalomyelitis.* J Exp Med, 2001. **193**(6): p. 713-26. PMC2193420 PMID: 11257138.
82. Chu, H.X., et al., *Role of CCR2 in inflammatory conditions of the central nervous system.* J Cereb Blood Flow Metab, 2014. **34**(9): p. 1425-9. PMC4158674 PMID: 24984897.
83. McGinley, A.M., et al., *Interleukin-17A Serves a Priming Role in Autoimmunity by Recruiting IL-1beta-Producing Myeloid Cells that Promote Pathogenic T Cells.* Immunity, 2020. **52**(2): p. 342-356 e6. PMID: 32023490.
84. Komuczki, J., et al., *Fate-Mapping of GM-CSF Expression Identifies a Discrete Subset of Inflammation-Driving T Helper Cells Regulated by Cytokines IL-23 and IL-1beta.* Immunity, 2019. **50**(5): p. 1289-1304 e6. PMID: 31079916.
85. Pare, A., et al., *IL-1beta enables CNS access to CCR2(hi) monocytes and the generation of pathogenic cells through GM-CSF released by CNS endothelial cells.* Proc Natl Acad Sci U S A, 2018. **115**(6): p. E1194-E1203. PMC5819409 PMID: 29358392.
86. Novartis Pharmaceuticals. *MCS110 in Patients With Pigmented Villonodular Synovitis (PVNS) or Giant Cell Tumor of the Tendon Sheath (GCTTS)*. 2012 [cited 2015 12/29/2015]; Available from: https://clinicaltrials.gov/ct2/show/NCT01643850.
87. Novartis Pharmaceuticals. *Efficacy Study of MCS110 Given With Carboplatin and Gemcitabine in Advanced Triple Negative Breast Cancer (TNBC)*. 2015 [cited 2015 12/29/2015]; Available from: https://clinicaltrials.gov/ct2/show/NCT02435680.
88. Novartis Pharmaceuticals. *A Phase I/II Open-label Study of MCS110 in Patients With Prostate Cancer and Bone Metastases*. 2008 [cited 2015 12/29/2015]; Available from: https://clinicaltrials.gov/ct2/show/NCT00757757.
89. Company, E.L.a. *A Study of IMC-CS4 in Subjects With Advanced Solid Tumors*. 2011 [cited 2015 12/29/2015]; Available from: https://clinicaltrials.gov/ct2/show/NCT01346358.

740 90. Cassier, P.A., et al., *CSF1R inhibition with emactuzumab in locally advanced diffuse-type tenosynovial giant cell*
741 *tumours of the soft tissue: a dose-escalation and dose-expansion phase 1 study.* Lancet Oncol, 2015. **16**(8): p.
742 949-56. PMID: 26179200.
743 91. Genovese, M.C., et al., *Results from a Phase IIA Parallel Group Study of JNJ-40346527, an Oral CSF-1R Inhibitor,*
744 *in Patients with Active Rheumatoid Arthritis despite Disease-modifying Antirheumatic Drug Therapy.* J
745 Rheumatol, 2015. **42**(10): p. 1752-60. PMID: 26233509.
746 92. Butowski, N., et al., *Orally administered colony stimulating factor 1 receptor inhibitor PLX3397 in recurrent*
747 *glioblastoma: an Ivy Foundation Early Phase Clinical Trials Consortium phase II study.* Neuro Oncol, 2016. **18**(4):
748 p. 557-64. PMC4799682 PMID: 26449250.
749 93. Tap, W.D., et al., *Structure-Guided Blockade of CSF1R Kinase in Tenosynovial Giant-Cell Tumor.* N Engl J Med,
750 2015. **373**(5): p. 428-37. PMID: 26222558.
751 94. Elmore, M.R., et al., *Colony-stimulating factor 1 receptor signaling is necessary for microglia viability, unmasking*
752 *a microglia progenitor cell in the adult brain.* Neuron, 2014. **82**(2): p. 380-97. PMC4161285 PMID: 24742461.
753 95. Goyal, A., et al., *Ultra-Fast Next Generation Human Genome Sequencing Data Processing Using DRAGEN Bio-IT*
754 *Processor for Precision Medicine.* Open Journal of Genetics, 2017. **Vol. 7**(No. 1). PMID.
755 96. Love, M.I., W. Huber, and S. Anders, *Moderated estimation of fold change and dispersion for RNA-seq data with*
756 *DESeq2.* Genome Biol, 2014. **15**(12): p. 550. PMC4302049 PMID: 25516281.

757

758

759

760

761

762

763

764

765

766

767

768

769

770

771

772 **FIGURES**

773 **Figure 1**

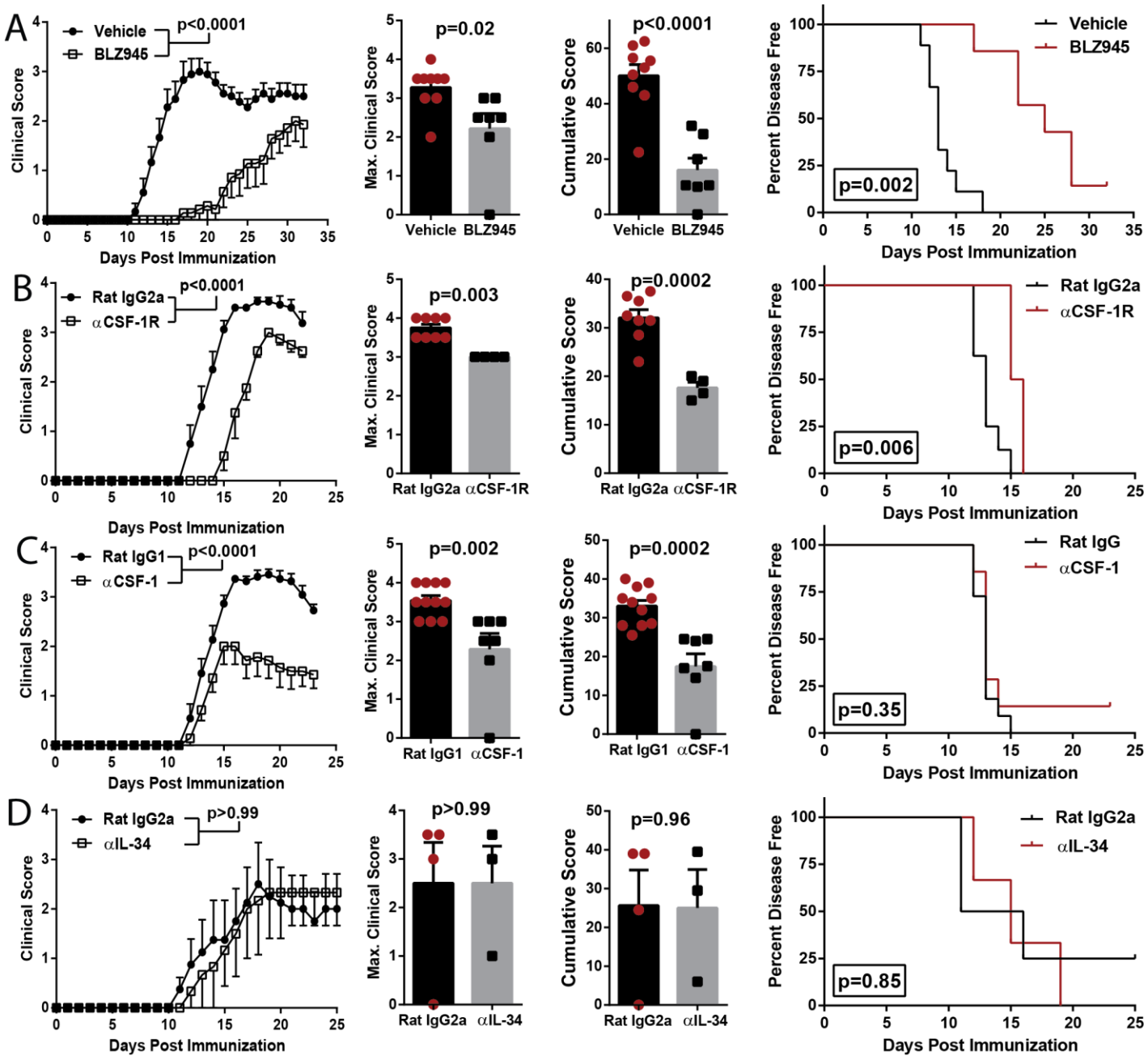

774

775

Figure 1: Blocking CSF-1R activity suppresses EAE. A-D) C57BL/6J mice were immunized with MOG_{35-55} for EAE induction. Clinical course, maximum and cumulative clinical scores, and Kaplan-Meier plots depicting percent of disease-free animals over time are shown. Significance for clinical course data was calculated by two-way repeated measures ANOVA. Significance for maximum and cumulative clinical scores was calculated by Student's *t* test. Error bars are S.E.M. Significance for Kaplan-Meier plots was calculated by comparing disease-free curves with the log-rank (Mantel-Cox) test. **A)** EAE animals treated orally with BLZ945 (n=9; 4 mg/day [1]) or vehicle (n=7; 20% Captisol) daily, starting from day of immunization. Data were compiled from two independent experiments. **B)** Treatment with anti-CSF-1R MAb (n=4) or control rat IgG2a (n=8). MAbs were i.p. injected every other day (400 µg per dose). **C)** Treatment with anti-CSF-1 MAb (n=7) or control rat IgG1 (n=11). MAbs were i.p. injected every other day (200 µg per dose). Data were compiled from two independent experiments. **D)** Treatment with anti-IL-34 MAb (n=3) or control rat IgG2a MAb (n=4). MAbs were i.p. injected every other day (100 µg per dose).

776

777

778

779

780

781

782

783

784

785

786

787

788

789

790

791

792

793

Figure 2

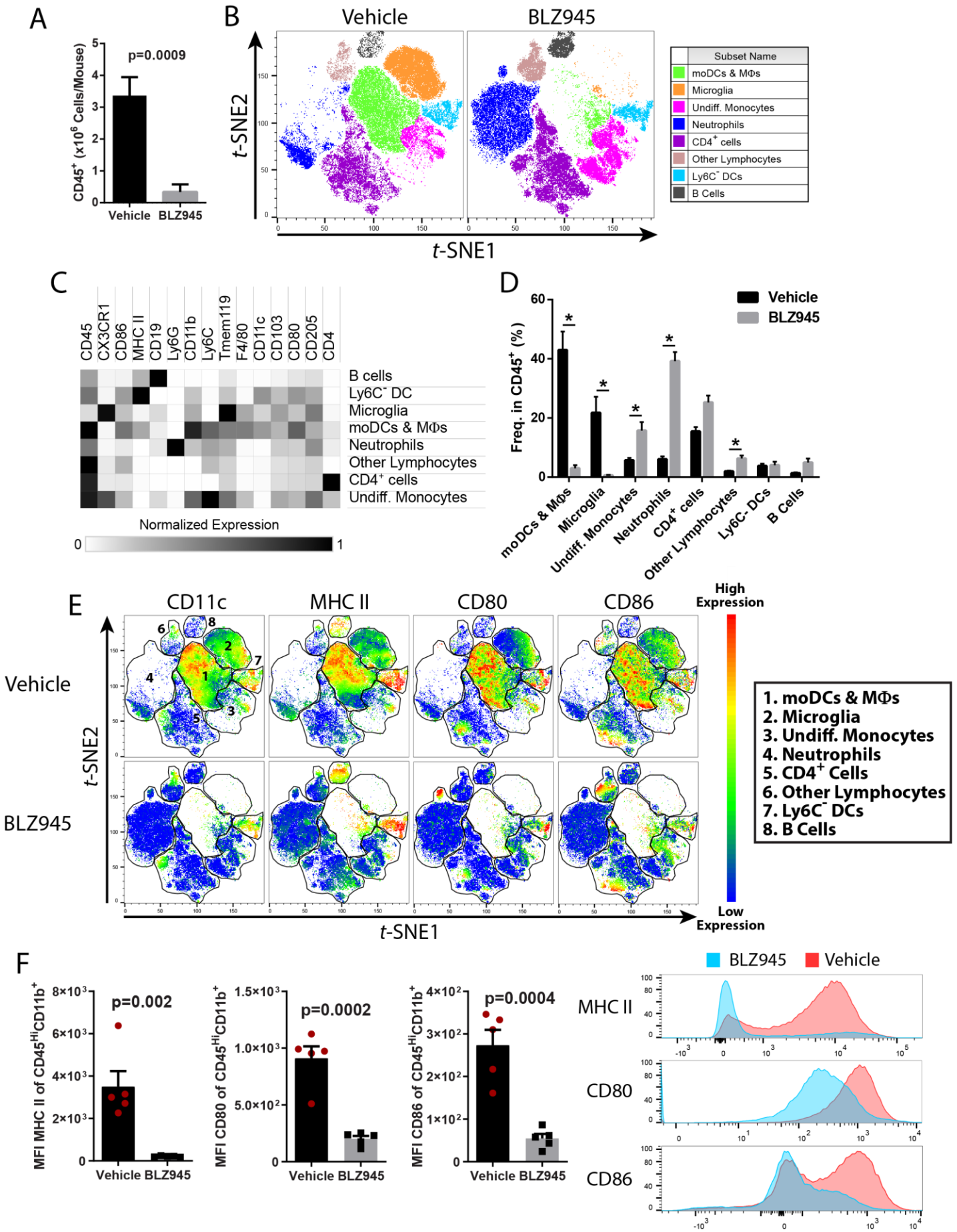
A
p=0.0009
CD45+ (x10^6 Cells/Mouse)
Vehicle
BLZ945
B
Vehicle
BLZ945
t-SNE2
t-SNE1
Subset Name
moDCs & MΦs
Microglia
Undiff. Monocytes
Neutrophils
CD4+ cells
Other Lymphocytes
Ly6C- DCs
B Cells
C
CD45
CX3CR1
CD86
MHC II
CD19
Ly6G
CD11b
Ly6C
Tmem119
F4/80
CD11c
CD103
CD80
CD205
CD4
B cells
Ly6C- DC
Microglia
moDCs & MΦs
Neutrophils
Other Lymphocytes
CD4+ cells
Undiff. Monocytes
Normalized Expression
0
1
D
Vehicle
BLZ945
Freq. in CD45+ (%)
moDCs & MΦs
Microglia
Undiff. Monocytes
Neutrophils
CD4+ cells
Other Lymphocytes
Ly6C- DCs
B Cells
E
CD11c
MHC II
CD80
CD86
High Expression
Low Expression
Vehicle
BLZ945
t-SNE2
t-SNE1
1. moDCs & MΦs
2. Microglia
3. Undiff. Monocytes
4. Neutrophils
5. CD4+ Cells
6. Other Lymphocytes
7. Ly6C- DCs
8. B Cells
F
p=0.002
MFI MHC II of CD45HiCD11b+
Vehicle BLZ945
p=0.0002
MFI CD80 of CD45HiCD11b+
Vehicle BLZ945
p=0.0004
MFI CD86 of CD45HiCD11b+
Vehicle BLZ945
BLZ945
Vehicle
MHC II
CD80
CD86

Figure 2: CSF-1R inhibition depletes myeloid APCs in the CNS of mice with EAE. C57BL/6J mice were immunized with MOG_{35-55} for EAE induction and treated orally with BLZ945 (4 mg/day) or vehicle control (20% captisol) daily, starting on the day of immunization. Mice were sacrificed on day 15 p.i., and brains and spinal cords were pooled for cell isolation. **A)** Numbers of CNS $CD45^+$ cells (n=7/group, combined from two independent experiments). **B)** *t*-SNE plot depicting clustering of $CD45^+$ cells (n=5 mice per group). moDCs and macrophages were defined by their expression of CD11b, CD11c, MHC II, CD80 and CD86. Microglia were defined as $CD45^+CD11b^+Tmem119^+CX3CR1^{Hi}$ cells. Undifferentiated monocytes were defined as $CD45^{Hi}Ly6C^{Hi}CD11c^-$ cells that were overall MHC $II^{Lo/Neg}$. Neutrophils were defined as $CD45^+CD11b^+Ly6G^{Hi}$. $CD4^+$ cells were defined as $CD45^+CD4^+$. Other lymphocytes were defined as $CD45^{Hi}SSC^{Lo}$. $Ly6C^-$ DCs were defined as $CD45^{Hi}CD11b^+CD11c^+MHCII^{Hi}Ly6C^-$ cells. B cells were defined as $CD45^+CD19^+$. **C)** Heatmap showing normalized expression of markers used to identify clusters. **D)** Quantification of clusters between vehicle and BLZ945-treated mice with EAE. **E)** Heat map of CD11c, MHC II, CD80 and CD86 expression among $CD45^+$ cells. **F)** MFI of MHC II, CD80 and CD86 among $CD45^{Hi}CD11b^+$ myeloid cells. Representative histograms showing fluorescence intensity of MHC II, CD80 and CD86 between vehicle- and BLZ945-treated animals is also shown. Y-axis is frequency of cells as normalized to mode. Significance was calculated with Student's *t* test. For D),* indicates a p-value < 0.02. Error bars are S.E.M.

796

797

798

799

800

801

802

803

804

805

806

807

808

809

810

811

Figure 3

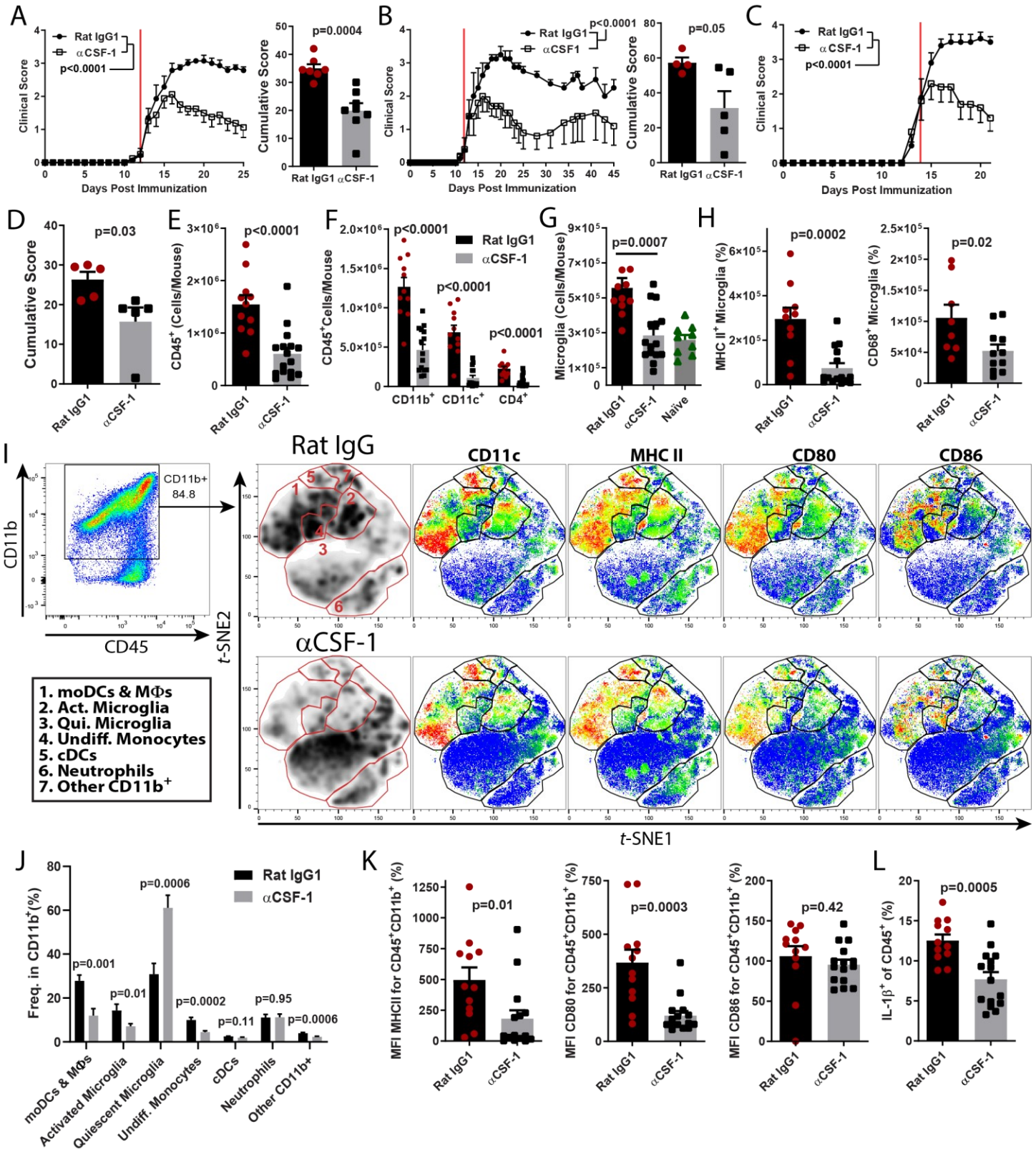
A
Rat IgG1
αCSF-1
p<0.0001
Clinical Score
Days Post Immunization
p=0.0004
Cumulative Score
Rat IgG1 αCSF-1
B
Rat IgG1
αCSF1
p<0.0001
Clinical Score
Days Post Immunization
p=0.05
Cumulative Score
Rat IgG1 αCSF-1
C
Rat IgG1
αCSF-1
p<0.0001
Clinical Score
Days Post Immunization
D
p=0.03
Cumulative Score
Rat IgG1
αCSF-1
E
p<0.0001
CD45+ (Cells/Mouse)
Rat IgG1
αCSF-1
F
p<0.0001
Rat IgG1
αCSF-1
p<0.0001
p<0.0001
CD45+Cells/Mouse
CD11b+
CD11c+
CD4+
G
p=0.0007
Microglia (Cells/Mouse)
Rat IgG1
αCSF-1
Naïve
H
p=0.0002
MHC II+ Microglia (%)
Rat IgG1
αCSF-1
p=0.02
CD68+ Microglia (%)
Rat IgG1
αCSF-1
I
CD11b+
84.8
CD11b
CD45
Rat IgG
CD11c
MHC II
CD80
CD86
αCSF-1
t-SNE2
t-SNE1
1. moDCs & MΦs
2. Act. Microglia
3. Qui. Microglia
4. Undiff. Monocytes
5. cDCs
6. Neutrophils
7. Other CD11b+
J
Rat IgG1
αCSF-1
Freq. in CD11b+(%)
p=0.001
p=0.01
p=0.0006
p=0.0002
p=0.11
p=0.95
p=0.0006
moDCs & MΦs
Activated Microglia
Quiescent Microglia
Undiff. Monocytes
cDCs
Neutrophils
Other CD11b+
K
MFI MHCII for CD45+CD11b+ (%)
p=0.01
Rat IgG1
αCSF-1
MFI CD80 for CD45+CD11b+ (%)
p=0.0003
Rat IgG1
αCSF-1
MFI CD86 for CD45+CD11b+ (%)
p=0.42
Rat IgG1
αCSF-1
L
p=0.0005
IL-1β+ of CD45+ (%)
Rat IgG1
αCSF-1

Figure 3: CSF-1 controls the population size of inflammatory myeloid cells in the CNS during EAE. A) Clinical course and cumulative score of mice with EAE treated with αCSF-1 MAb starting after disease onset (n=7 per group; compiled from 2 independent experiments). Red line denotes day that treatment was started. Mice were treated with 200 μg MAb per day. **B)** Clinical course and cumulative scores of mice treated long term with αCSF-1 MAb. Mice were treated daily until day 25, and then every other day for the duration of the experiment. **C-D)** Clinical course and cumulative score for mice treated with αCSF-1 MAb, starting at clinical score of 2.0 (n=4-5 per group). **E-L)** Characterization of immune cells from the CNS of control MAb- and αCSF-1 MAb-treated mice. **E)** Number of $CD45^+$ cells. **F)** Numbers of $CD11b^+$, $CD11c^+$ and $CD4^+$ cells. **G)** Numbers of $CD45^+CD11b^+CX3CR1^{Hi}Tmem119^+$ microglia in control-treated, αCSF-1 MAb-treated, and naïve mice. **H)** Numbers of MHC II^+ and $CD68^+$ microglia in control MAb- and αCSF-1 MAb-treated mice. **I)** *t*-SNE analysis of $CD45^+CD11b^+$ cells. moDCs and macrophages were defined by their expression of CD11b, CD11c, MHC II, CD80 and CD86. Activated microglia were defined as $CD45^+CD11b^+Tmem119^+CX3CR1^{Hi}MHCII^+CD68^{+/-}$ cells. Quiescent microglia were defined as $CD45^+CD11b^+Tmem119^+CX3CR1^{Hi}MHCII^-CD68^-$. Undifferentiated monocytes were defined as $CD45^{Hi}Ly6C^{Hi}CD11c^-$ cells that were overall MHC $II^{Lo/Neg}$. Neutrophils were defined as $CD45^+CD11b^+Ly6G^{Hi}$. $CD4^+$ cells were defined as $CD45^+CD4^+$. cDCs were defined as $CD45^{Hi}CD11b^+CD11c^+MHCII^{Hi}Ly6C^-CD26^+$ cells. Other $CD11b^+$ cells expressed CD11c and CX3CR1 but did not express markers for antigen presentation. **J)** Quantification of clusters from I). **K)** Median fluorescence intensity of MHC II, CD80 and CD86 in $CD45^+CD11b^+$ cells. **L)** Frequency of IL-1β^+ cells among $CD45^+$ cells. Significance was calculated with unpaired Student's *t* test. Error bars are S.E.M. Significance for clinical course was calculated by two-way ANOVA.

814

815

816

817

818

819

820

821

822

823

824

825

826

827

Figure 4

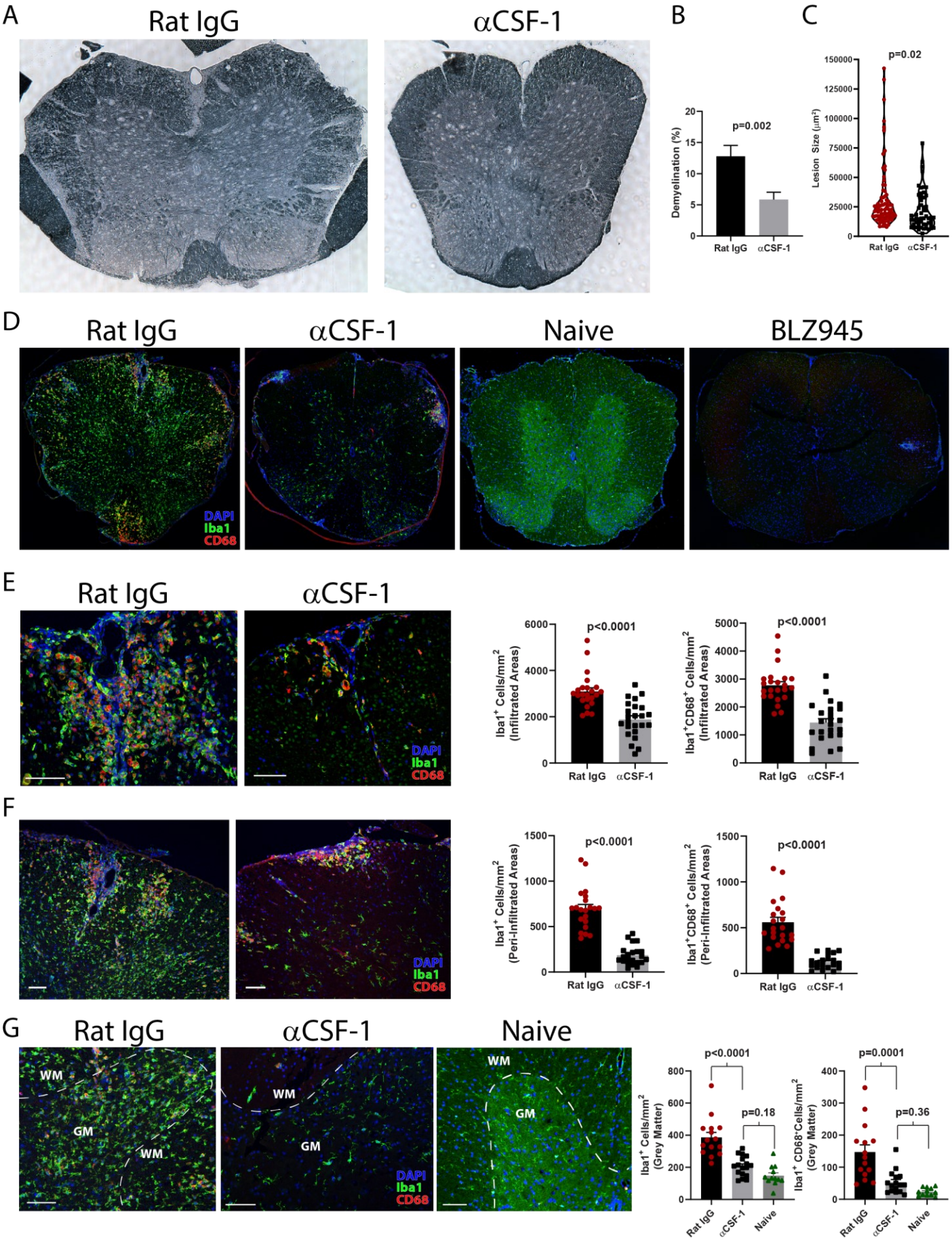
A
Rat IgG
αCSF-1
B
Demyelination (%)
p=0.002
Rat IgG
αCSF-1
C
Lesion Size (μm²)
p=0.02
Rat IgG
αCSF-1
D
Rat IgG
αCSF-1
Naive
BLZ945
DAPI
Iba1
CD68
E
Rat IgG
αCSF-1
DAPI
Iba1
CD68
Iba1⁺ Cells/mm² (Infiltrated Areas)
p<0.0001
Iba1⁺CD68⁺ Cells/mm² (Infiltrated Areas)
p<0.0001
Rat IgG
αCSF-1
F
DAPI
Iba1
CD68
Iba1⁺ Cells/mm² (Peri-Infiltrated Areas)
p<0.0001
Iba1⁺CD68⁺ Cells/mm² (Peri-Infiltrated Areas)
p<0.0001
Rat IgG
αCSF-1
G
Rat IgG
αCSF-1
Naive
WM
GM
WM
WM
GM
DAPI
Iba1
CD68
WM
GM
Iba1⁺ Cells/mm² (Grey Matter)
p<0.0001
p=0.18
Iba1⁺ CD68⁺Cells/mm² (Grey Matter)
p=0.0001
p=0.36
Rat IgG
αCSF-1
Naive

Figure 4: Anti-CSF1 treatment reduces lesion burden without depleting quiescent microglia. A) Sudan black stained spinal cord sections from rat IgG- and anti-CSF-1-treated mice with EAE sacrificed on day 17-19 p.i. (n=5 mice per group). Spinal cords were split into 4 pieces of equal length, and 1 section from each piece is included in the analysis. **B)** Degree of demyelination expressed as a percentage of demyelinated white matter. **C)** Violin plot showing demyelinating lesion size in rat IgG- and anti-CSF-1-treated mice. **D)** Confocal microscopy of spinal cord sections stained with DAPI and Abs against Iba1 and CD68 from rat IgG-, anti-CSF-1-, and BLZ945-treated EAE mice, and naïve mice. **E)** Representative images and quantification of cell density of $Iba1^+$ and $Iba1^+CD68^+$ cells within lesions infiltrated with immune cells from rat IgG- and anti-CSF-1-treated mice. **F)** Representative images and quantification of cell density of $Iba1^+$ and $Iba1^+CD68^+$ cells within a 100 µm-wide area surrounding lesions infiltrated with immune cells. **G)** Representative images and quantification of cell density of $Iba1^+$ and $Iba1^+CD68^+$ cells in grey matter of rat IgG- or anti-CSF-1-treated and naïve mice. All scale bars are 100 µm. For E) and F), individual lesions from 5 mice per group are analyzed. Significance was calculated with unpaired Student's *t* test. Error bars are S.E.M. Significance for comparisons between more than two groups was calculated by one-way ANOVA.

830

831

832

833

834

835

836

837

838

839

840

841

842

843

844

845

846

847 **Figure 5**

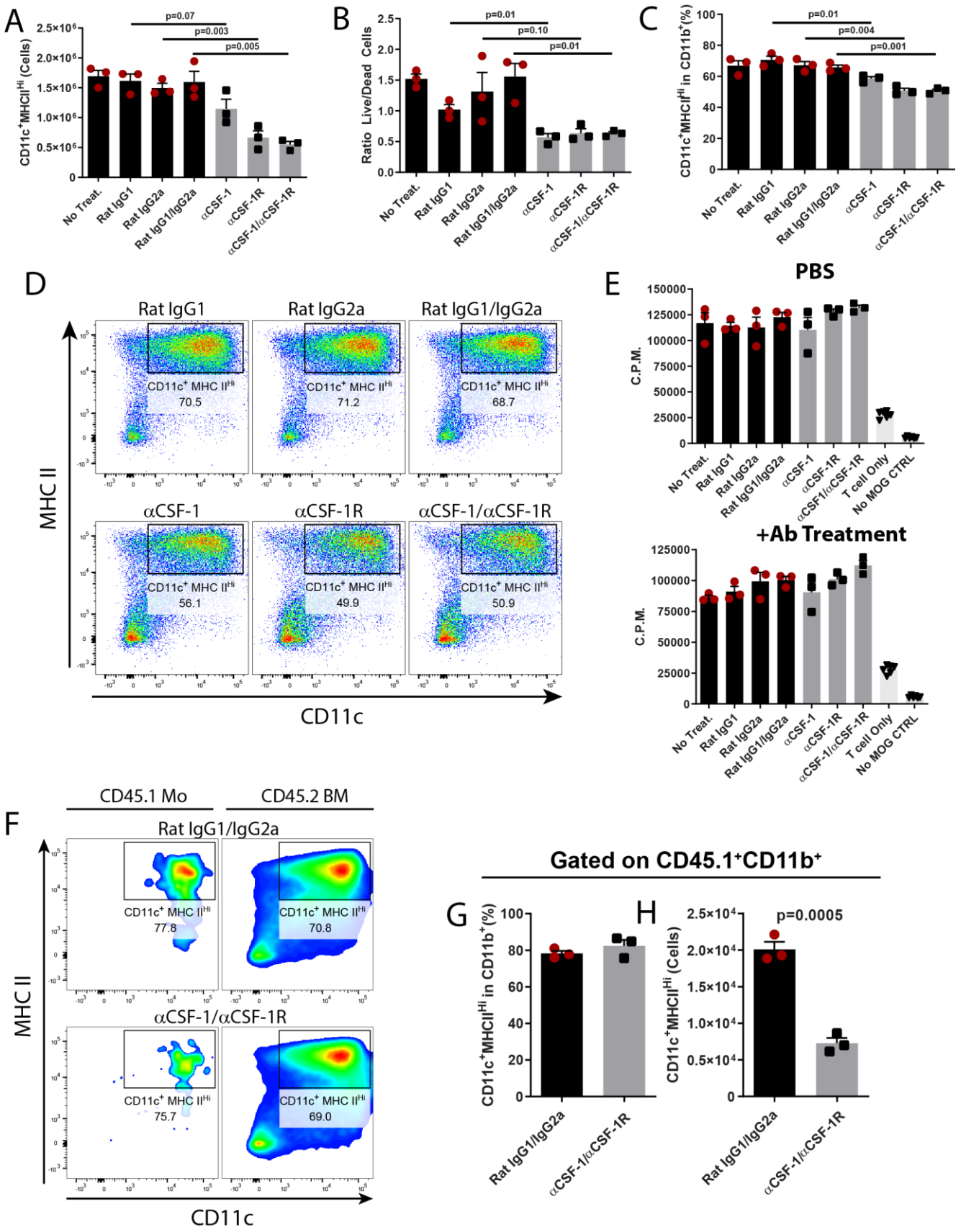

848

Figure 5: CSF-1R signaling promotes survival and proliferation of moDCs, but not their APC function. BM cells were cultured in media supplemented with GM-CSF and IL-4 for 7 days in the presence of either control MAbs, or anti-CSF1 and anti-CSF-1R MAbs. BMDCs were then matured by stimulation with LPS for 24 h in the presence of the MAbs. **A)** Number of $CD11c^{+}MHCII^{Hi}$ cells in culture after GM-CSF + IL-4 treatment for 7 days. **B)** Ratio of Live/Dead cells after 24 h LPS treatment. **C-D)** Frequency of $CD11c^{+}MHCII^{Hi}$ cells after GM-CSF + IL-4 treatment for 7 days. **E)** Co-culture of LPS-matured BMDCs with $CD4^{+}$ T cells from 2D2 mice and MOG_{35-55} peptide (25 μg/mL). Co-cultures either did, or did not contain control and neutralizing MAbs against CSF-1 and CSF-1R. Proliferation was measured using [^{3}H]Thymidine incorporation. C.P.M. = counts per minute. **F)** Monocytes were purified from the BM of CD45.1 mice and mixed with total BM of CD45.2 mice, then cultured as described above with control or anti-CSF1/anti-CSF-1R MAbs. Flow cytometry depicting CD11c and MHC II expression in $CD45.1^{+}CD11b^{+}$ and $CD45.2^{+}CD11b^{+}$ cells is shown. **G)** Frequency, and **H)** number of $CD11c^{+}MHC\ II^{Hi}$ cells among $CD45.1^{+}CD11b^{+}$ cells. Technical replicates for 1 of 2 independent experiments with similar results are shown. Statistical significance was calculated using two-way unpaired *t* test. Error bars are S.E.M.

849

850

851

852

853

854

855

856

857

858

859

860

861

862

863

864

865

Figure 6

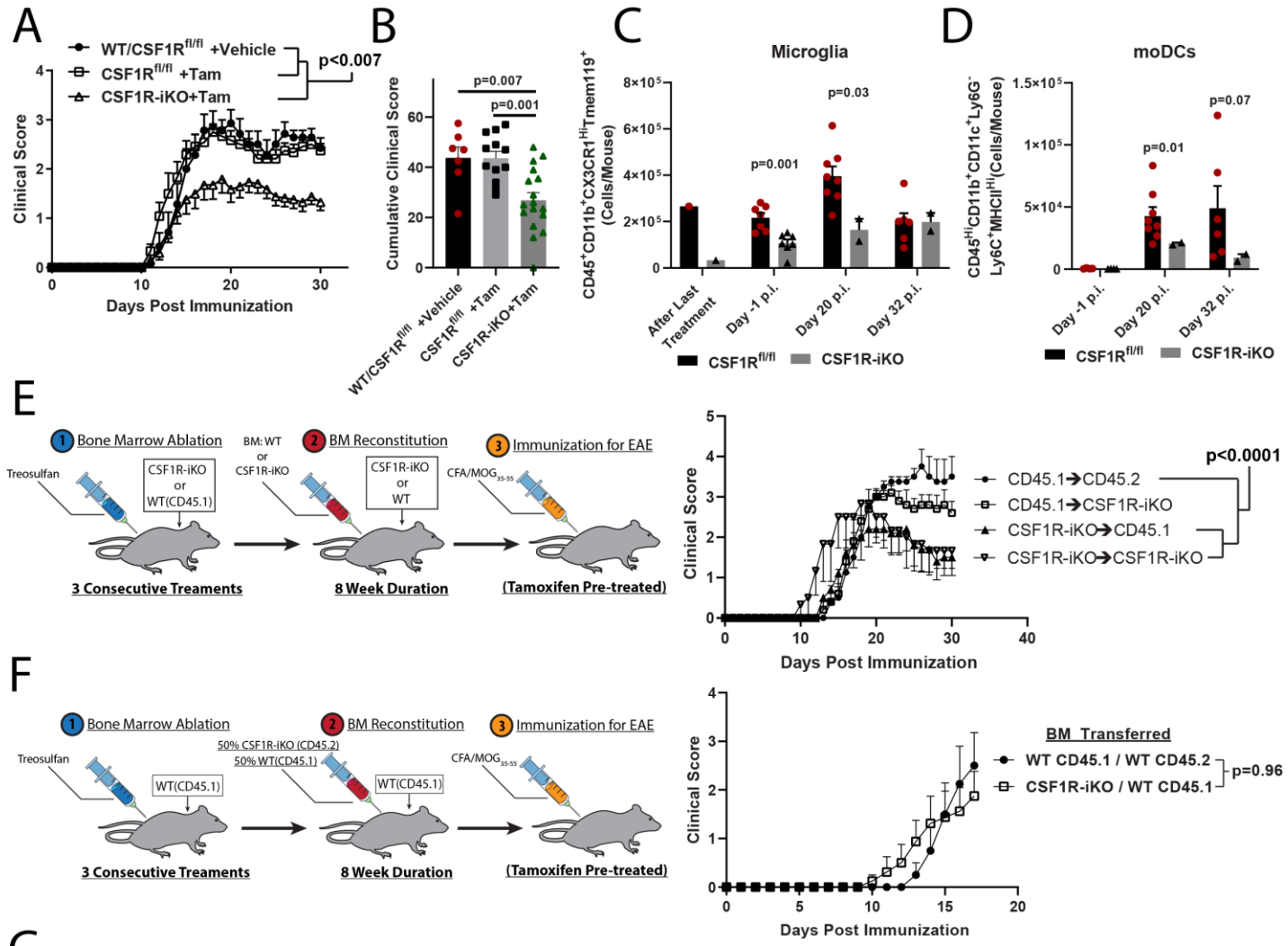
A
WT/CSF1R fl/fl +Vehicle
CSF1R fl/fl +Tam
CSF1R-iKO+Tam
p<0.007
Clinical Score
Days Post Immunization
B
p=0.007
p=0.001
Cumulative Clinical Score
WT/CSF1R fl/fl +Vehicle
CSF1R fl/fl +Tam
CSF1R-iKO+Tam
C
Microglia
p=0.001
p=0.03
After Last Treatment
Day -1 p.i.
Day 20 p.i.
Day 32 p.i.
CSF1R fl/fl
CSF1R-iKO
D
moDCs
p=0.01
p=0.07
Day -1 p.i.
Day 20 p.i.
Day 32 p.i.
CSF1R fl/fl
CSF1R-iKO
E
1 Bone Marrow Ablation
Treosulfan
CSF1R-iKO or WT(CD45.1)
3 Consecutive Treaments
BM: WT or CSF1R-iKO
2 BM Reconstitution
CSF1R-iKO or WT
8 Week Duration
3 Immunization for EAE
CFA/MOG35-55
(Tamoxifen Pre-treated)
p<0.0001
CD45.1➔CD45.2
CD45.1➔CSF1R-iKO
CSF1R-iKO➔CD45.1
CSF1R-iKO➔CSF1R-iKO
Clinical Score
Days Post Immunization
F
1 Bone Marrow Ablation
Treosulfan
WT(CD45.1)
3 Consecutive Treaments
2 BM Reconstitution
50% CSF1R-iKO (CD45.2)
50% WT(CD45.1)
WT(CD45.1)
8 Week Duration
3 Immunization for EAE
CFA/MOG35-55
(Tamoxifen Pre-treated)
BM Transferred
WT CD45.1 / WT CD45.2
CSF1R-iKO / WT CD45.1
p=0.96
Clinical Score
Days Post Immunization
G
WT (CD45.1)
CSF1R-iKO (CD45.2)
Ly6C+MHCII+ 62.7
Ly6C+MHCII+ 35.6
MHC II
Ly6C
WT (CD45.1)
WT (CD45.2)
Ly6C+MHCII+ 50.4
Ly6C+MHCII+ 50.0
CSF1R-iKO/WT BM
p=0.01
WT/WT BM
p=0.21
WT (CD45.1)
CSF1R-iKO (CD45.2)
WT (CD45.1)
WT (CD45.2)

Figure 6. BM-derived immune cells are the major contributors to CSF-1R-dependent pathology A) Comparison between vehicle (n=7) and tamoxifen-treated (n=17) *Csf1r*$^{fl/fl}$ mice and tamoxifen-treated CSF1R-iKO mice (n=12). **B)** Quantification of cumulative score from C). Significance for clinical course determined by two-way repeated measures ANOVA, and by unpaired Student's *t* test for cumulative scores. **C)** Time course showing numbers of microglia and **D)** moDCs in tamoxifen-treated *Csf1r*$^{fl/fl}$ and CSF1R-iKO mice. Significance was calculated by unpaired Student's *t* test **E)** BM was ablated with treosulfan, and 10^7 WT or CSF1R-iKO BM cells were i.v. transferred into either WT or CSF1R-iKO recipients. After 8 weeks reconstitution, mice were treated with tamoxifen and immunized for EAE. Right panel shows clinical course of EAE. Numbers of mice per group were 4, 5, 5, 3 for group listed in legend from top to bottom. **F)** Mixed BM chimera experiments. BM was ablated as in G, then equal numbers of WT and CSF1R-iKO BM cells were co-transferred to recipients (total cell number transferred = 10^7 cells/mouse) via i.v. injection. After reconstitution period, mice were treated with tamoxifen, rested, and then immunized for EAE induction. Significance for BM chimera experiments was calculated by two-way repeated measures ANOVA. **G)** Quantification of frequency of monocyte-derived APCs among CD11b$^+$ cells from mixed BM chimeras in H). Significance was determined by two-tailed paired *t* test.

870

871

872

873

874

875

876

877

878

879

880

881

882

883

884

885

886

887 **SUPPLEMENTAL MATERIALS**

888

889 **MATERIALS AND METHODS**

890 **Flow Cytometry**

891 Isolated cells were stimulated with PMA (500 ng/mL; Sigma Aldrich), ionomycin (50 ng/mL; Sigma Aldrich), and
892 1 µL/mL Golgiplug (BD Biosciences) for 4 h at 37°C. After stimulation, cells were washed with PBS containing
893 3% FBS (v/v). Cell surface antigens were stained with Abs in 100 µL of PBS/3% FBS for 20-30 min at 4°C. Cells
894 were then washed and fixed with 100 µL Fix and Perm Medium A (Thermo Fisher) for 20 min at room temperature
895 and washed again. Cells were permeabilized with Fix and Perm Medium B (Thermo Fisher) and stained with
896 Abs against intracellular antigens in 100 µL Fix and Perm Medium B and 100 µL PBS/3%FBS for 1 h. Cells were
897 then washed twice, resuspended in 500 µL PBS and analyzed on a BD FACSAria Fusion flow cytometer (BD
898 Biosciences).

899

900 **Isolation of Immune Cells from the CNS**

901 Mice were anesthetized and blood was removed by perfusion with 60 mL PBS. Spinal cord was flushed out of
902 the spinal column with PBS. Brains and spinal cords were pooled and cut manually into small pieces in 700 µL
903 Liberase TL dissolved in RPMI at 0.7 mg/mL (Roche) then incubated at 37°C for 30 min before reaction was
904 quenched using complete media containing FBS. Tissue was homogenized by pushing through a 100 µm sterile
905 filter with syringe plunger. Homogenate was centrifuged at 1500 RPM (300 x g) for 5 min and resuspended in
906 25 mL of 70% 1x Percoll-PBS (90% Percoll, 10% 10x PBS). 25 mL of 30% Percoll-PBS was gently overlayed
907 onto the 70% layer and was centrifuged at 2000 RPM without brake at room temperature for 30 min. Cells that
908 pooled at the interface of 30/70% layers and the majority of the 30% layer were then collected, diluted with PBS
909 or media and centrifuged at 1500 RPM (300 x g) for 5 min.

910

911

912

913 **Antibody Titer Measurement**

914 Serum was collected from peripheral blood of animals treated with Rat IgG_{2A} (Clone: 2A3; Bio X Cell), anti-CSF1
915 MAb (Clone: 5A1; Bio X Cell), anti-CSF-1R MAb (Clone: AFS98; Bio X Cell), anti-IL-34 MAb (Clone: 780310,
916 Novus Biologicals). 96-well ELISA plates were coated with the same MAb that was used to treat animals
917 overnight at room temperature and blocked with 1% BSA for 2 h. Plates were washed and incubated with serum
918 for 1 h and washed. Anti-Mouse IgG-HRP conjugate secondary Ab (Jackson Immunolabs) was used to detect
919 the presence of anti-Rat IgG response by measuring absorbance at 450 nm and subtracting absorbance at 540
920 nm.

921

922 **Library Preparation and RNA-seq Analyses**

923 Next-generation sequencing libraries were prepared using the Illumina TruSeq Stranded Total RNA library
924 preparation kit, with high quality RNA (RIN >= 8.7) and 200 ng of input RNA. Libraries were assessed for quality
925 using the PerkinElmer Labchip GX and qPCR using the Kapa Library Quantification Kit and the Life Technologies
926 Viia7 Real-time PCR instrument. Libraries were diluted to 2 nM and sequenced in a paired-end (2 x 100bp),
927 dual-indexed format on the Illumina HiSeq2500 using the High Output v4 chemistry.

928 RNA-seq reads were demultiplexed into sample-specific fastq files and aligned to the mm10 reference genome
929 using the DRAGEN genome pipeline [95] to produce BAM files. Generated BAM files were read into R statistical
930 computing environment and gene counts were obtained using the Rsubread package, producing a feature/gene
931 counts matrix. Differential expression analysis was performed using the R/Bioconductor package DESeq2, which
932 uses a negative binomial model [96]. Analysis was performed using standard thresholds and parameters while
933 filtering genes with low mean normalized counts. Further downstream analysis was performed using the
934 Ingenuity Pathway Analysis (IPA) and GSEA software using the normalized read count table. Additionally,
935 differentially expressed genes ($p<0.01$) were entered into the DAVID utility for functional annotation and analyzed
936 for gene ontology terms for biological processes and for KEGG pathway terms [58, 59].

937

938

939 **Tamoxifen Treatment**

940 Tamoxifen (Sigma) was resuspended in corn oil (Sigma) to 20 mg/mL by heating in a 37ºC water bath and
941 vortexing. For tamoxifen treatment via i.p. injection, 2 mg of tamoxifen was injected per day for a total of 5
942 injections. Mice were then rested for 14-21 days before further manipulation. For tamoxifen treatment via oral
943 gavage, mice were treated 5 times with 5 mg of tamoxifen per day, then rested for 7 days.

944

945 **Immunohistochemistry and Immunofluorescence Microscopy**

946 Animals were perfused with 50 mL PBS followed by 40 mL cold paraformaldehyde (PFA) solution. The spinal
947 column was then removed and placed in PFA overnight. The day after perfusion, tissue was transferred to 30%
948 sucrose in PBS and allowed to incubate overnight, or until tissue had sunk to the bottom of the tube. Spinal cord
949 was then dissected from the spinal column, cut into 4 pieces of approximately equal length and embedded in
950 OCT. The entire spinal cord was sectioned into 10 µm-thick coronal sections, skipping 100 µm between each
951 section. Prior to staining, sections were immersed in PBS for 10 min to remove residual OCT. For Sudan black
952 staining, sections were stained by immersion for 30 min in a 10 mg/mL solution of Sudan black prepared in 70%
953 ethanol. Following staining, slides were decolorized by immersion in a 0.1% Triton-X100 in PBS solution for 30
954 min. For immunofluorescence experiments, slides were blocked using 10% Normal Goat Serum with 0.1%
955 sodium azide (Thermo Fisher) for 30 min. Primary Abs for Iba1 (1:500 dilution, SySy, Cat# 234 006), and CD68
956 (1:100 dilution, Thermo Fisher, Clone: FA-11) were diluted in 10% Normal Goat Serum with 0.3% Triton-X100.
957 Slides were stained with primary Abs overnight at 4ºC, then washed 3 times with PBS for 5 min. Secondary Abs
958 (Thermo Fisher) were diluted 1:1000 and slides were stained for 1 h. Slides were then washed 3 times with PBS,
959 mounted with ProLong™ Diamond Antifade Mountant with DAPI (Thermo Fisher) and imaged using a Nikon AR1
960 confocal microscope at the Thomas Jefferson University Imaging core facility.

961

962 **Analysis of Immunofluorescence Microscopy**

963 Demyelination in Sudan black-stained spinal cord sections was determined by dividing total demyelinated area
964 of white matter by total white matter area, using NIS elements software (Nikon). Immunofluorescence images

965 were analyzed using Slidebook 6 software (Intelligent Imaging Innovations). Quantification of cell density was
966 performed by masking cell nuclei by fluorescent thresholding. Touching nuclei were separated by applying the
967 watershed algorithm at 25% aggressiveness and then again at 50% after removal of small objects. Errors in
968 object identification or over-segmentation caused by the watershed algorithm were then corrected manually.
969 Features of spinal cord sections were manually masked (e.g. lesions, grey matter, etc.) and cells not belonging
970 to that feature were discarded by only keeping cells that overlapped with the feature mask. Object IDs were then
971 assigned to individual cells and mean pixel intensity per object was determined for each channel. A threshold
972 intensity value was then assigned for each channel and used to determine positivity for that marker. The number
973 of positive cells was then divided by the area of that feature to determine cell density.

974

975 **Western Blot**

976 Cells were re-suspended in a RIPA lysis buffer supplemented with a protease inhibitor cocktail (Sigma-Aldrich).
977 30 mg proteins diluted with Laemmli buffer and loaded onto 8%–14% polyacrylamide gels. Protein
978 concentrations were measured with bicinchoninic acid (BCA) assay (Pierce). Anti-CSF-1R (Abcam) and mouse
979 anti-β actin (Sigma) were used as primary antibodies.

980

981 **Bone Marrow-Derived DC Culture**

982 Bone marrow (BM) was isolated from tibia and femurs of mice, and BM cells were cultured at 1 x 10^6 cells per
983 mL in a total volume of 10 mL in petri dishes with GM-CSF (20 ng/mL) + IL-4 (20 ng/mL) for 4 days. On the 4th
984 day, 5 mL of media was removed from the plates, cells were pelleted by centrifugation and resuspended in 5 mL
985 fresh media containing GM-CSF and IL-4. The cell suspension was added back to the original petri dishes and
986 cultured for an additional 3 days. To induce a mature DC phenotype, cells were washed, replated in fresh media
987 containing LPS (300 ng/mL) and cultured for 72 h. For cultures involving monocytes, $CD11b^+$ cells were isolated
988 from BM cell suspension of $CD45.1^+$ mice by MACS positive selection (Miltenyi Biotec), after which $Ly6C^{Hi}Ly6G^-$
989 monocytes were sorted on a FACSAria Fusion instrument (BD Biosciences). Isolated monocytes were then
990 added to $CD45.2^+$ total BM cell cultures.

991 **Co-culture of DCs and T cells and Proliferation Assay**

992 For proliferation assays, 4 x 10^4 DCs were co-cultured with 1.6 x 10^5 2D2 $CD4^+$ T cells in 96-well U-bottom tissue
993 culture plates. Cells were stimulated with MOG_{35-55} peptide (25 μg/mL) for 72 h. At approximately 60 h after
994 starting the culture, 1 µCi of [^{3}H]Thymidine (Perkin-Elmer) was added to each well in a volume of 50 µL. Cells
995 were harvested 24 h later and counts per minute (C.P.M.) measured in MicroBeta2 beta counter (Perkin-Elmer).

996

997 **Bone Marrow Chimeras**

998 Treosulfan (L-threitol-1,4-dimethanesulfonate; a generous gift from Medac Germany) was resuspended in sterile
999 water at a concentration of 50 mg/mL and administered by i.p. injection over 3 consecutive days at 2000 mg/kg
1000 per dose. Mice were then rested for 72-96 h before i.v. transfer of 10^7 BM cells.

1001
1002
1003
1004
1005
1006
1007
1008
1009
1010
1011
1012
1013
1014
1015
1016
1017
1018
1019
1020

SUPPLEMENTAL FIGURES

Supplemental Figure 1

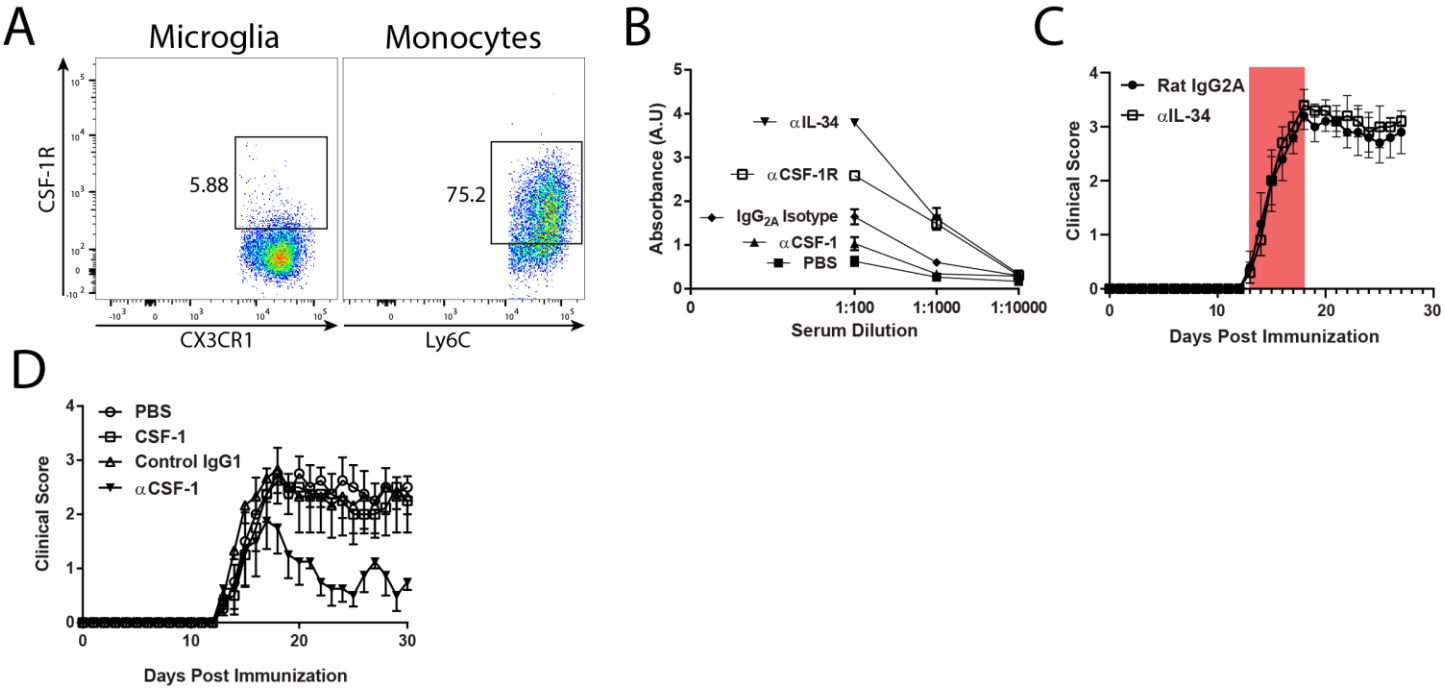

Supplemental Figure 1: A) C57BL6/J mice were immunized with MOG_{35-55} and treated with anti-CSF1 MAb (200 µg, every other day), control rat IgG1 MAb (200 µg, every other day), recombinant mouse CSF-1 (4 µg per dose, given on days 4, 8 ,12 ,16 p.i.) or PBS by i.p. injection. **B)** Serum Ab titers of mice with EAE treated with MAbs against IL-34 (n=3), CSF-1R (n=3), IgG2a isotype (n=4), CSF1 (n=3), and control animals treated with PBS (n=6). Error bars are standard error from the mean. **C)** Flow cytometry plots depicting staining of $CD45^{+}CD11b^{+}CX3CR1^{Hi}$ microglia and $CD45^{Hi}CD11b^{+}Ly6G^{-}Ly6C^{Hi}$ monocytes for CSF-1R with the AFS98 MAb. **D)** C57BL6/J mice were immunized with MOG_{35-55} and treated with anti-IL-34 MAb (55 µg per day, i.p) for the period indicated by the red box.

Supplemental Figure 2

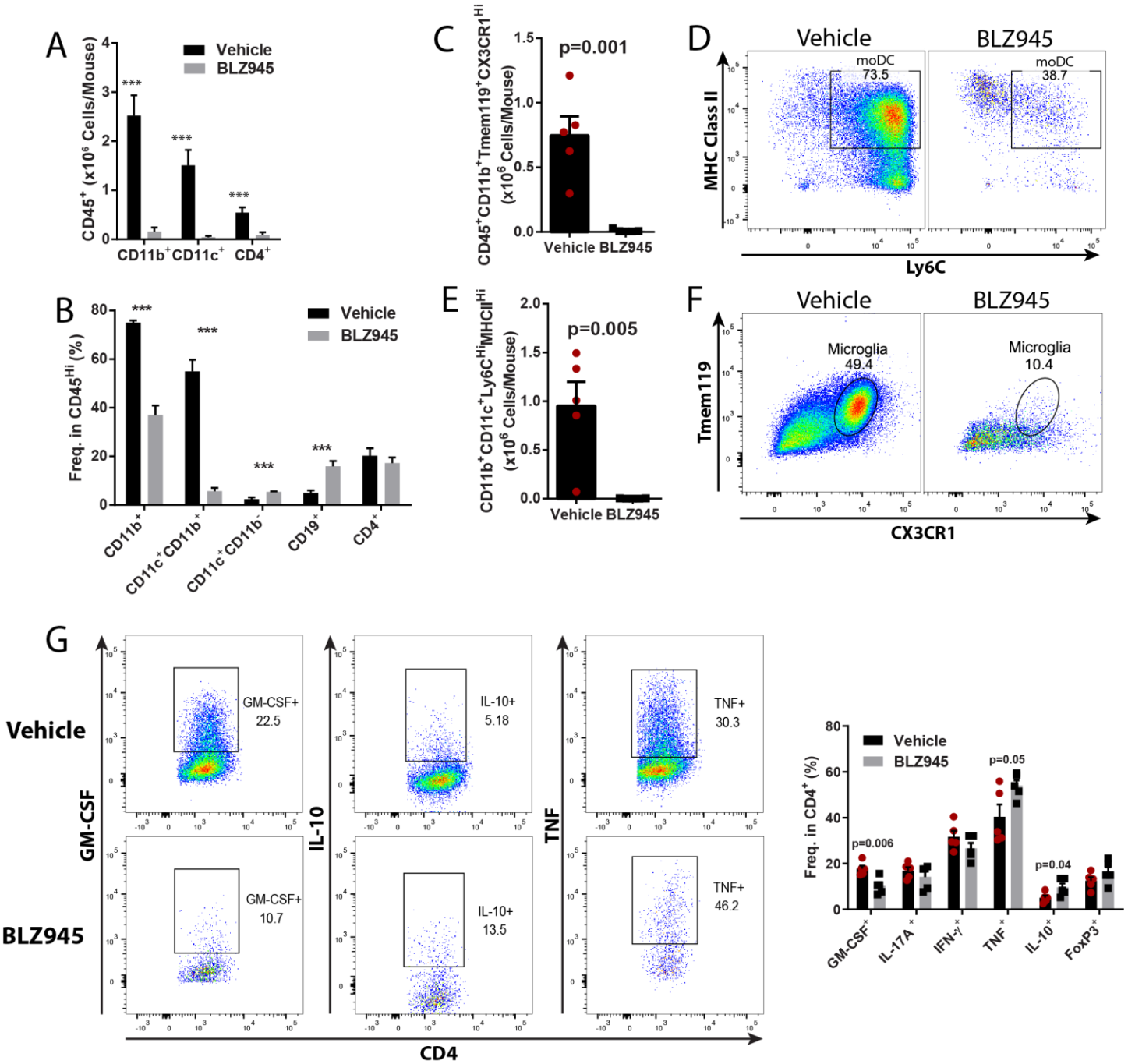

Supplemental Figure 2: Inhibition of CSF-1R signaling alters both myeloid and T cell compartments in the CNS of EAE mice. C57BL/6J mice were immunized with MOG_{35-55} for EAE induction and treated orally with BLZ945 (200 mg/kg/day) or vehicle control (20% captisol) daily, starting on the day of immunization. Mice were sacrificed on day 15 p.i., and pooled brain and spinal cords of each mouse were used for cell isolation (n=5/group). **A)** Numbers of $CD11b^+$, $CD11c^+$ and $CD4^+$ cells. **B)** Frequency of $CD11b^+$, $CD11b^+CD11c^+$ $CD11b^+CD11c^-$, $CD19^+$, and $CD4^+$ cells in $CD45^{Hi}$ cells. **C-F)** Numbers of $CD45^+CD11b^+Tmem119^+CX3CR1^{Hi}$ microglia and $CD45^{Hi}CD11b^+Ly6C^{Hi}MHCII^{Hi}$ moDCs. **G)** Quantification of GM-CSF, IL-17A, IFN-γ, TNF, IL-10 and FoxP3 expression by $CD4^+$ cells from the CNS. Significance was calculated with Student's *t* test. Error bars are S.E.M.

Supplemental Figure 3

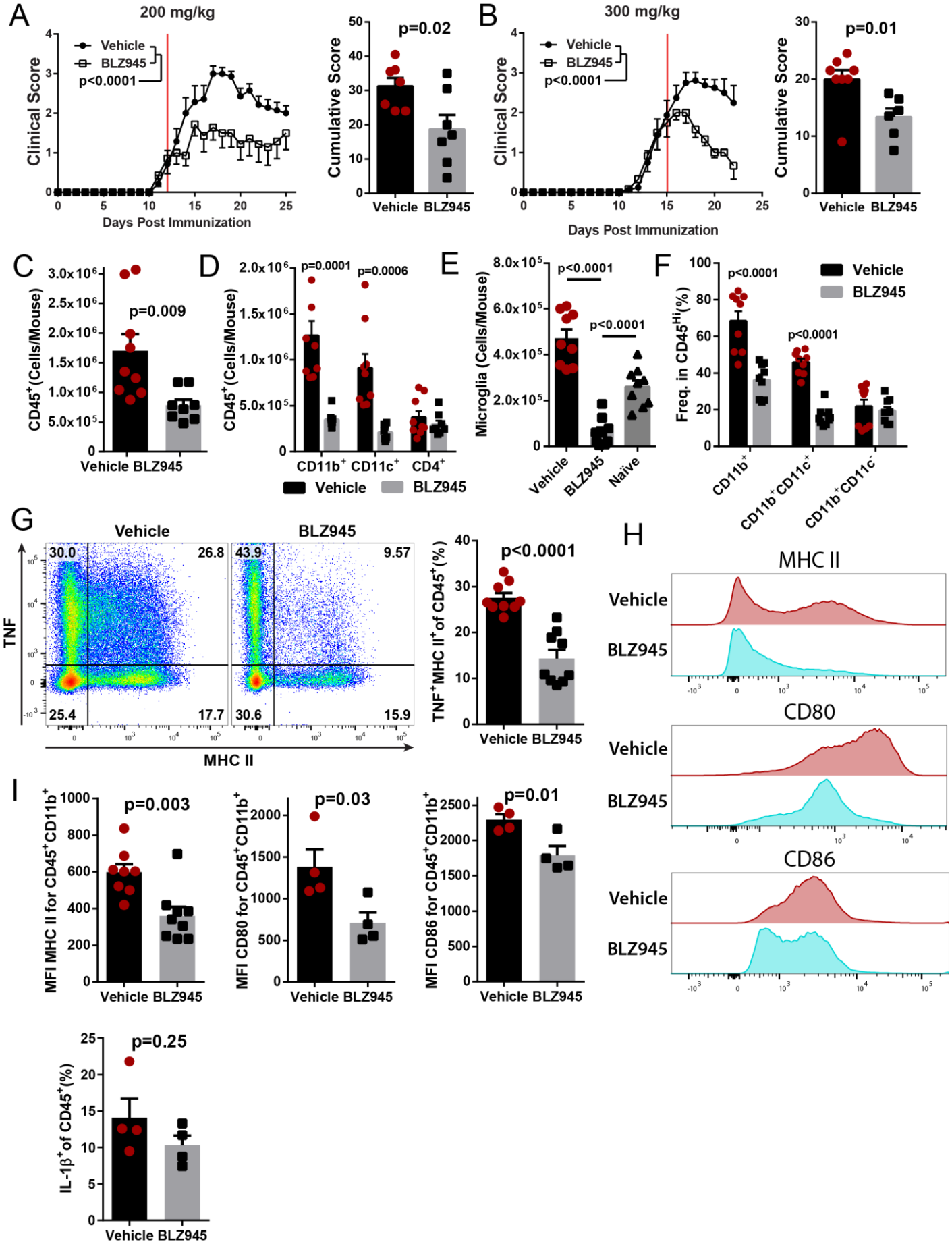

Supplemental Figure 3. BLZ945 suppresses ongoing clinical EAE, and reduces the number of myeloid APCs in the CNS. C57BL/6J mice were immunized and allowed to develop clinical signs of EAE before treatment with BLZ945 (n=7) or vehicle (n=8). Treatments were given once per day by oral gavage. **A)** Clinical course and cumulative score for mice treated with 200 mg/kg BLZ945 starting at a clinical score of ~1. Red line indicates start of treatment. **B)** Mice treated with 300 mg/kg BLZ945 (n=6) or vehicle (n=8), starting at a clinical score of ~2. A) and B) were compiled from two independent experiments. Significance for clinical course determined by two-way repeated measures ANOVA, and by unpaired Student's *t* test for cumulative scores. **C-I)** Analysis of the CNS (pooled brain and spinal cords) by flow cytometry. **C)** Number of $CD45^{+}$ cells. **D)** Number of $CD45^{+}$ cells that also expressed CD11b, CD11c, or CD4. **E)** Number of $CD45^{Lo}CD11b^{+}CX3CR1^{Hi}$ microglia. Naïve mice are untreated WT C57BL/6J mice that were not immunized or otherwise manipulated. **F)** Frequency of $CD45^{Hi}$ cells that also express CD11b and/or CD11c. **G)** TNF and MHC II expression in $CD45^{+}$ cells. **H-I)** Expression of MHC II, CD80 and CD86 in $CD45^{+}CD11b^{+}$ cells. Significance for C-I) was calculated by unpaired Student's *t* test. P-value corrections for multiple comparisons was performed by false discovery rate approach with Q=0.01 as a cutoff. Error bars are S.E.M.

1044
1045
1046
1047
1048
1049
1050
1051
1052
1053
1054
1055
1056
1057
1058
1059
1060
1061
1062
1063
1064
1065
1066
1067
1068
1069

Supplemental Figure 4

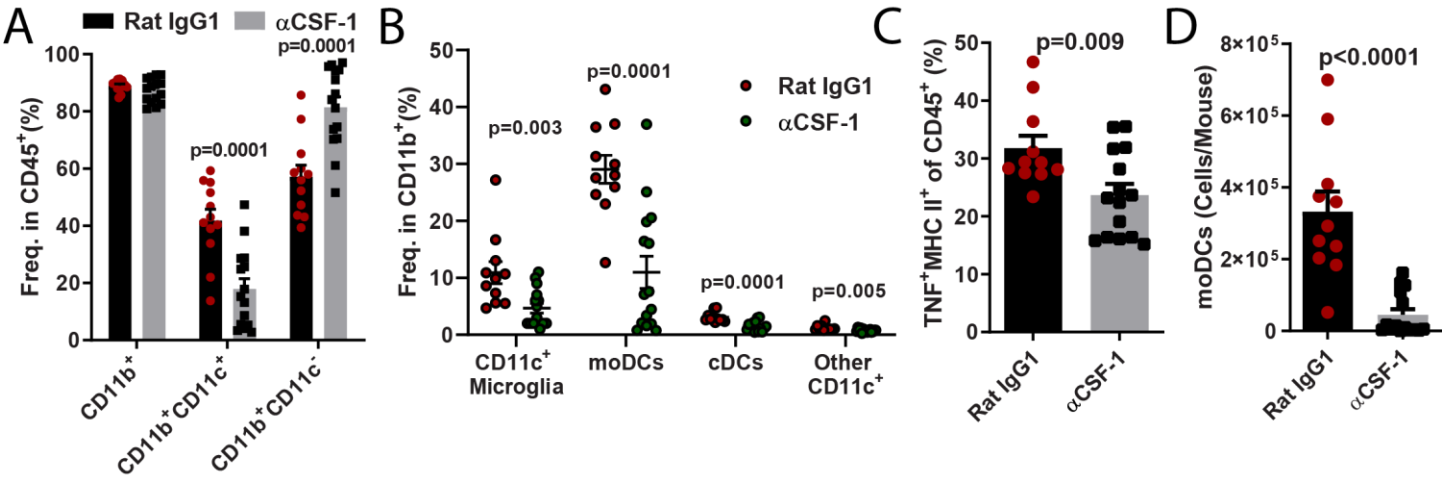

Supplemental Figure 4: Anti-CSF-1 treatment reduces numbers of DCs in the CNS of mice with EAE. A) Frequency of CD11b$^+$, CD11b$^+$CD11c$^+$, CD11b$^+$CD11c$^-$ cells among CD45$^+$ cells from the CNS of mice with EAE treated with either anti-CSF-1 or control MAb. **B)** Frequency of CD11c$^+$ microglia (CD45$^+$CD11b$^+$CX3CR1^{Hi}Tmem119$^+$), moDCs (CD45^{Hi}CD11b$^+$CD11c$^+$Ly6G$^-$Ly6C^{Hi}MHCII^{Hi}), cDCs (CD45^{Hi}CD11b$^+$CD11c$^+$CD26$^+$Ly6C$^-$MHCII$^+$) and other CD11c$^+$ cells among CD11b$^+$ cells. **C)** Number of CD45^{Hi}CD11b$^+$CD11c$^+$Ly6G$^-$Ly6C^{Hi}MHCII^{Hi} moDCs. **D)** Frequency of TNF$^+$MHC II$^+$ cells among CD45$^+$ cells. Significance was calculated with unpaired Student's *t* test. Error bars are S.E.M.

Supplemental Figure 5

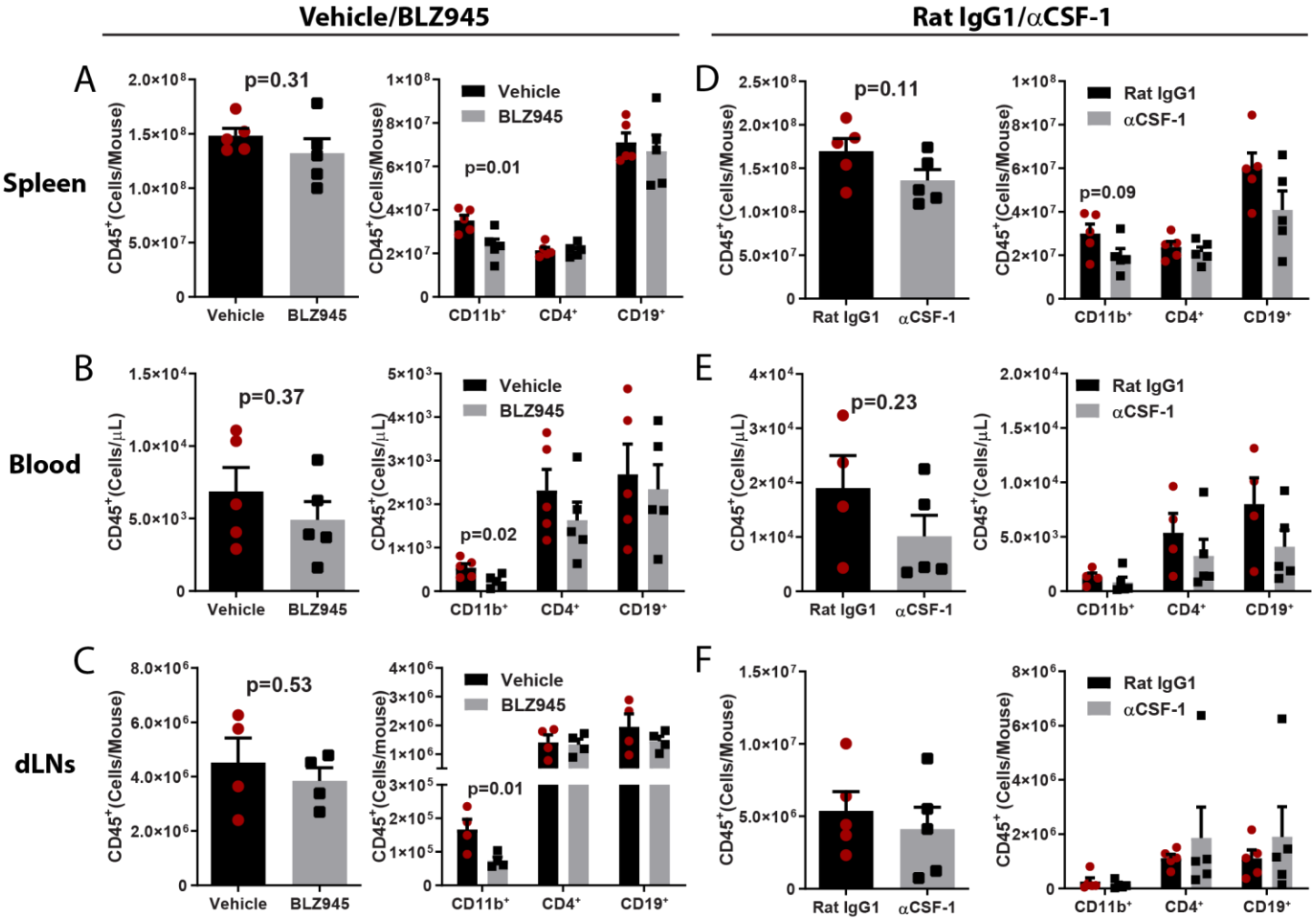

Supplementary Figure 5: Immune response in peripheral lymphoid organs of BLZ945- and anti-CSF-1-treated mice on day 8 p.i. A-C) BLZ945- and vehicle-treated mice (n=5 per group). Number of CD45⁺, CD11b⁺, CD4⁺ and CD19⁺ cells in **A)** spleen, **B)** blood, and **C)** dLN. **E-F)** Same quantification as in A-C), but for anti-CSF-1- and rat IgG1 control MAb-treated mice. Statistical significance was calculated using two-way unpaired *t* test. Error bars are standard S.E.M.

Supplemental Figure 6

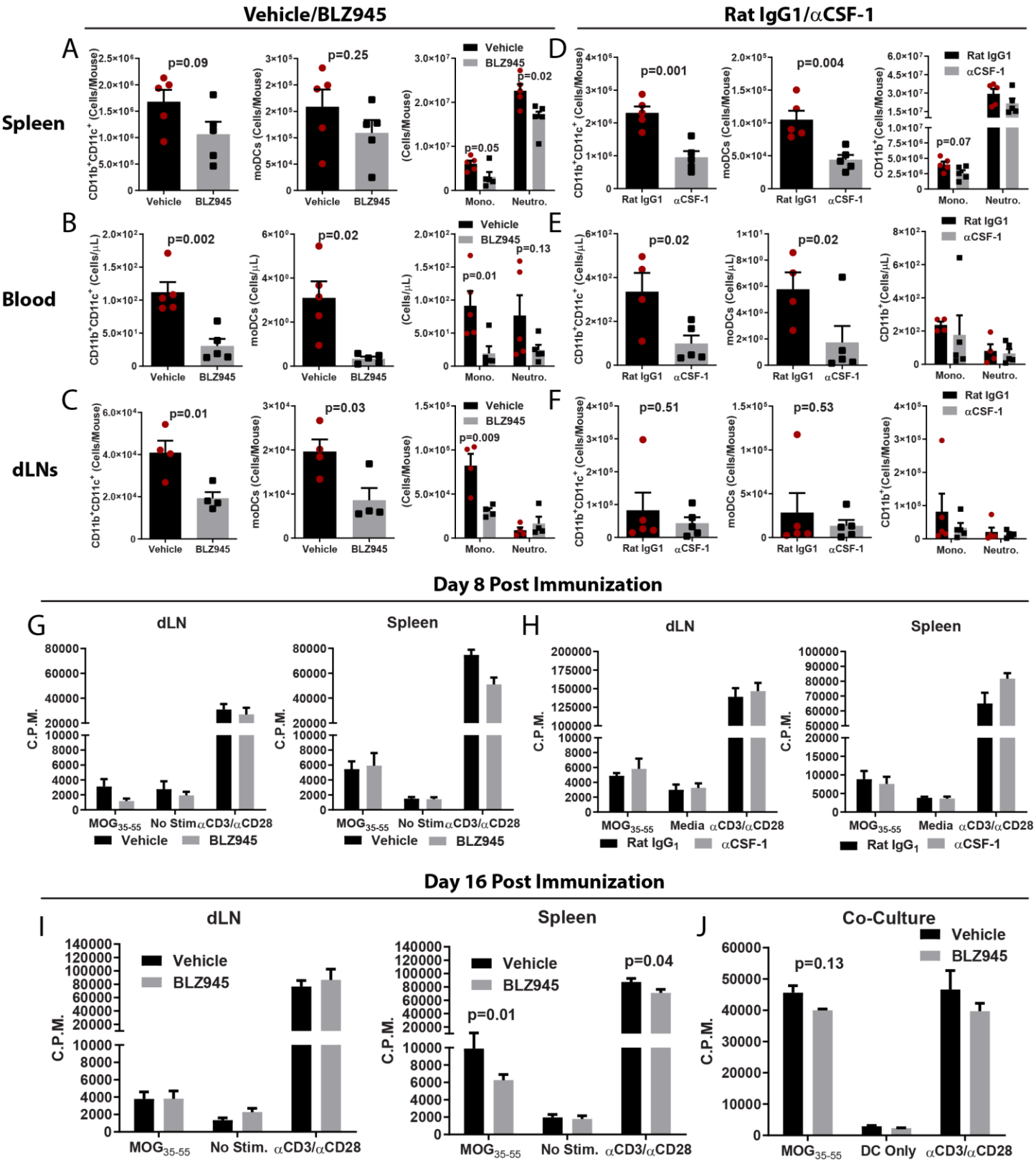

Supplemental Figure 6: CSF-1R inhibition depletes myeloid DCs and monocytes in peripheral lymphoid compartments. Characterization of immune cells in the spleen, blood and dLNs from MOG_{35-55}-immunized mice sacrificed on day 8 p.i.. **A-C)** BLZ945- and vehicle-treated mice (n=5 per group). Numbers of $CD11b^{+}CD11c^{+}$, moDCs, monocytes and neutrophils in **A)** spleen, **B)** blood, and **C)** dLN. **E-F)** Same quantification as in A-C) but for anti-CSF-1- and rat IgG1 control MAbs-treated mice. **G)** [^{3}H]Thymidine proliferation assay for MOG_{35-55}-stimulated splenocytes and dLNs cells from BLZ945- and vehicle-treated mice harvested on day 8 p.i. **H)** Same analyses as in G), but for anti-CSF-1- and rat IgG1 control MAb-treated mice. **I)** [^{3}H]Thymidine proliferation assay for MOG_{35-55}-stimulated splenocytes and dLNs cells from BLZ945- and vehicle-treated mice harvested on day 16 p.i. **J)** $CD11c^{+}$ cells in splenocytes from BLZ945- and vehicle-treated mice harvested on day 8 p.i. $CD11c^{+}$ cells were isolated by magnetic bead sorting and mixed in a 1:10 ratio with $CD4^{+}$ T cells isolated from splenocytes of 2D2 mice, and stimulated with MOG_{35-55} for 72 h. Proliferation was then measured by [^{3}H]Thymidine incorporation assay. Statistical significance was calculated using two-way unpaired *t* test. Error bars are S.E.M.

Supplemental Figure 7

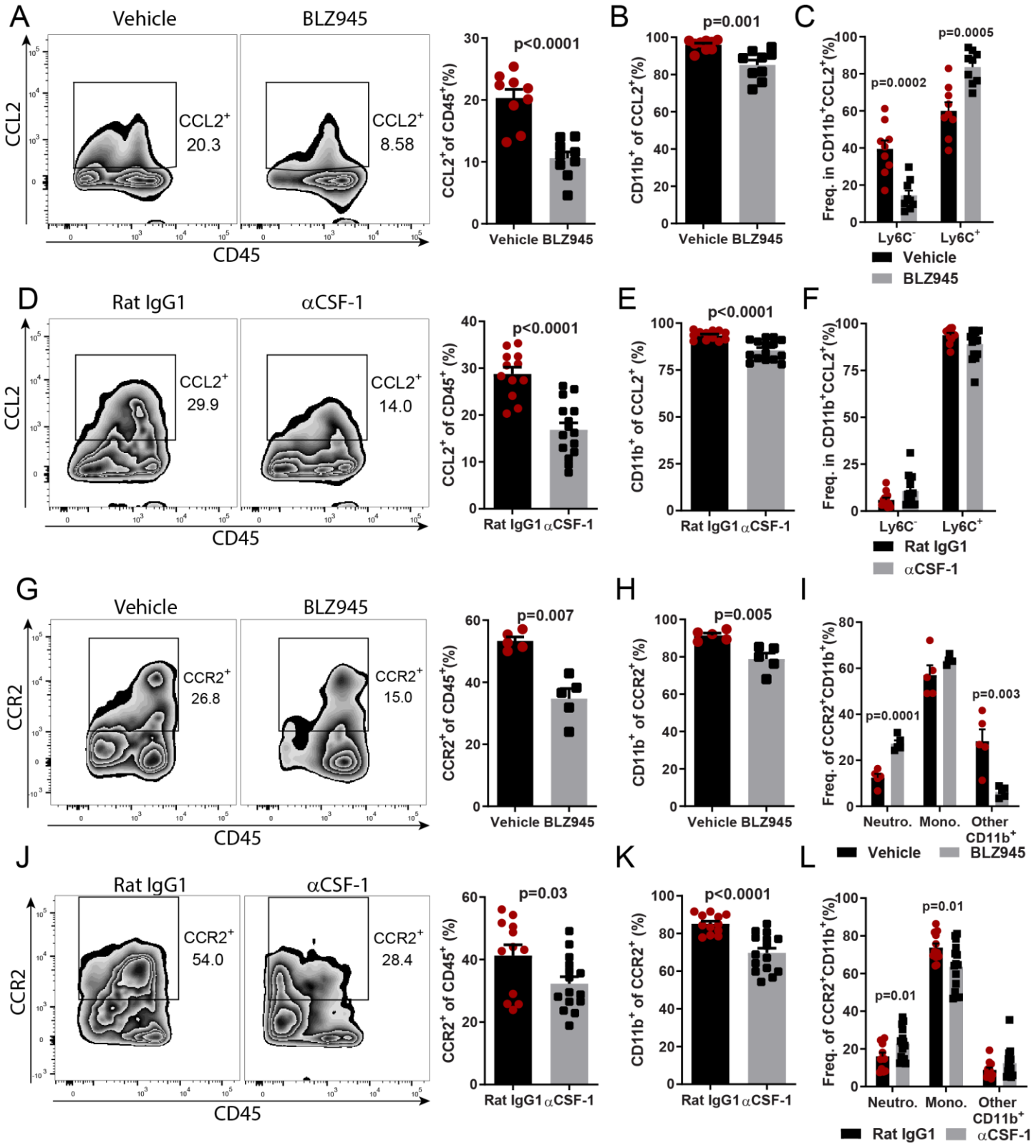

Supplemental Figure 7: Blocking CSF-1R or CSF-1 reduces numbers of CCL2⁺ and CCR2⁺ myeloid cells in the CNS during EAE. A) Frequency of CCL2⁺ cells among CD45⁺ cells in the CNS of BLZ945- and vehicle-treated mice (n=9 per group) sacrificed after 6 days of treatment, at day 20 p.i.. **B)** CD11b⁺ cells among CCL2⁺ cells. **C)** Frequency of Ly6C⁺ and Ly6C⁻ cells among CD11b⁺CCL2⁺ cells. **D)** Frequency of CCL2⁺ cells among CD45⁺ cells from the CNS of anti-CSF-1- and control MAb-treated mice (n=12-15 per group), sacrificed after 6 days of treatment, at 17 days p.i.. **E)** CD11b⁺ cells among CCL2⁺ cells. **F)** Frequency of Ly6C⁺ and Ly6C⁻ cells among CD11b⁺CCL2⁺ cells. **G)** Frequency of CCR2⁺ cells among CD45⁺ cells from the CNS of BLZ945- and vehicle-treated mice from A). **H)** CD11b⁺ cells among CCL2⁺ cells. **I)** Frequency of neutrophils ($CD45^{Hi}CD11b^{+}Ly6G^{Hi}Ly6C^{Int}$), monocytes/monocyte-derived cells ($CD45^{Hi}CD11b^{+}Ly6G^{Neg/Lo}Ly6C^{+}$) and other CD11b⁺ cells among CCR2⁺CD11b⁺ cells. **J)** Frequency of CCR2⁺ cells among CD45⁺ cells from the CNS of anti-CSF-1- and control MAb-treated mice from D). **K)** CD11b⁺ cells among CCL2⁺ cells. **L)** Frequency of neutrophils ($CD45^{Hi}CD11b^{+}Ly6G^{Hi}Ly6C^{Int}$), monocytes/monocyte-derived cells ($CD45^{Hi}CD11b^{+}Ly6G^{Neg/Lo}Ly6C^{+}$) and other CD11b⁺ cells among CCR2⁺CD11b⁺ cells. Statistical significance was calculated using two-tailed unpaired *t* test. Error bars are S.E.M.

Supplemental Figure 8

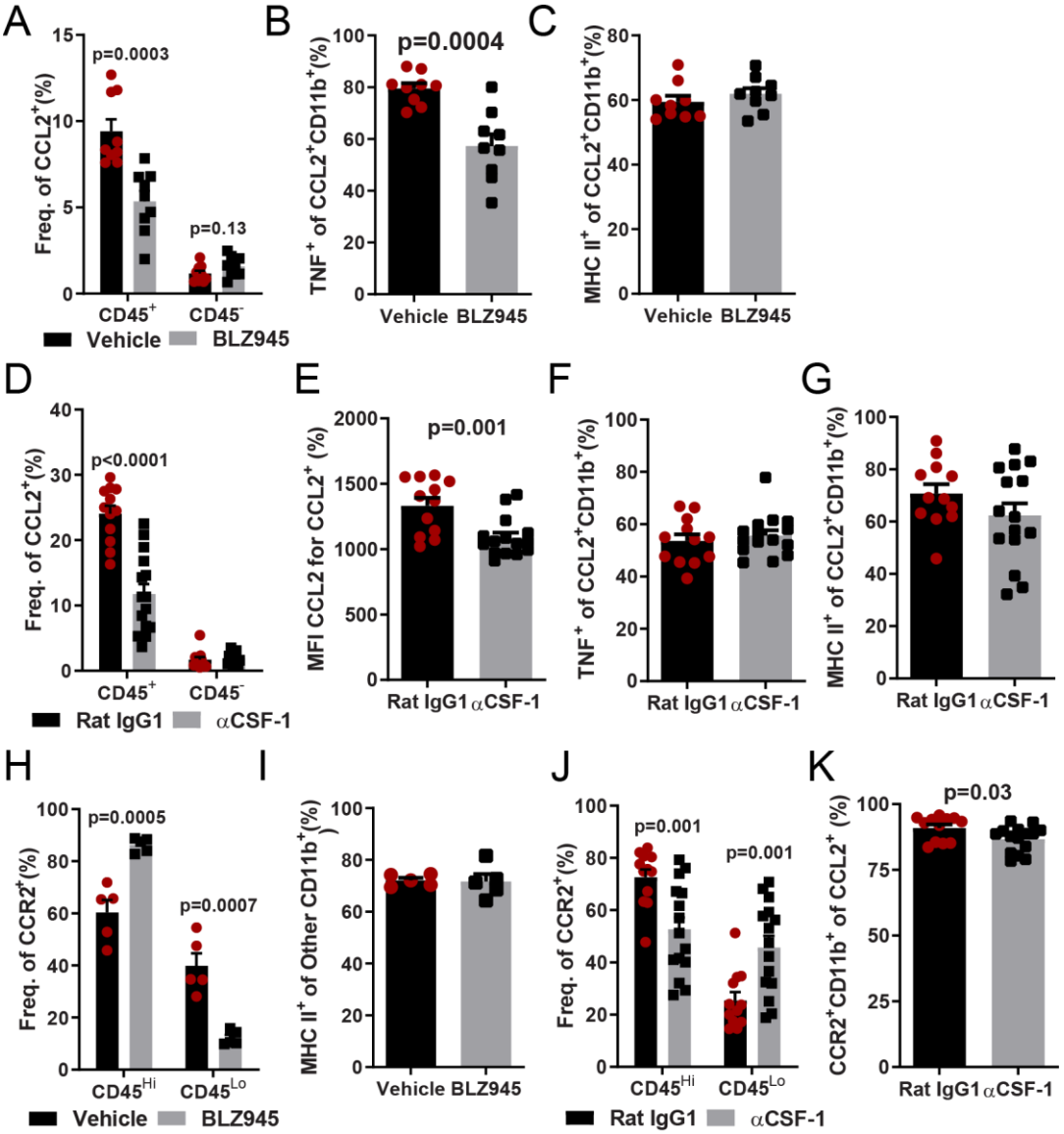

Supplemental Figure 8. CCL2⁺ and CCR2⁺ cells are primarily composed of inflammatory myeloid cells. Frequency of CCL2⁺CD45⁺ and CCL2⁺CD45⁻ cells among mononuclear cells isolated from the CNS of BLZ945- and vehicle-treated mice with EAE. **B)** Frequency of TNF⁺, and **C)** MHC II⁺ cells among CCL2⁺CD11b⁺ cells. **D)** Frequency of CCL2⁺CD45⁺ and CCL2⁺CD45⁻ cells among mononuclear cells isolated from the CNS of anti-CSF-1- and control MAb-treated EAE mice. **E)** MFI of CCL2⁺ cells among CD45⁺CCL2⁺ cells. **F)** Frequency of TNF⁺, and **G)** MHC II⁺ cells among CCL2⁺CD11b⁺ cells. **H)** Frequency of CCR2⁺ cells among CD45⁺ cells that were either CD45^{Hi} or. CD45^{Lo} in BLZ945- or vehicle-treated EAE mice. **I)** Percentage of MHC II⁺ among "Other CD11b⁺ cells" from Fig. 7B. **J)** Frequency of CCR2⁺ cells among CD45⁺ cells that were either CD45^{Hi} or CD45^{Lo} in anti-CSF-1- or control MAb-treated mice. **K)** Frequency of CCR2⁺CD11b⁺ cells among CCL2⁺ cells. Statistical significance was calculated with two-tailed unpaired *t* test. Error bars are S.E.M.

Supplemental Figure 9

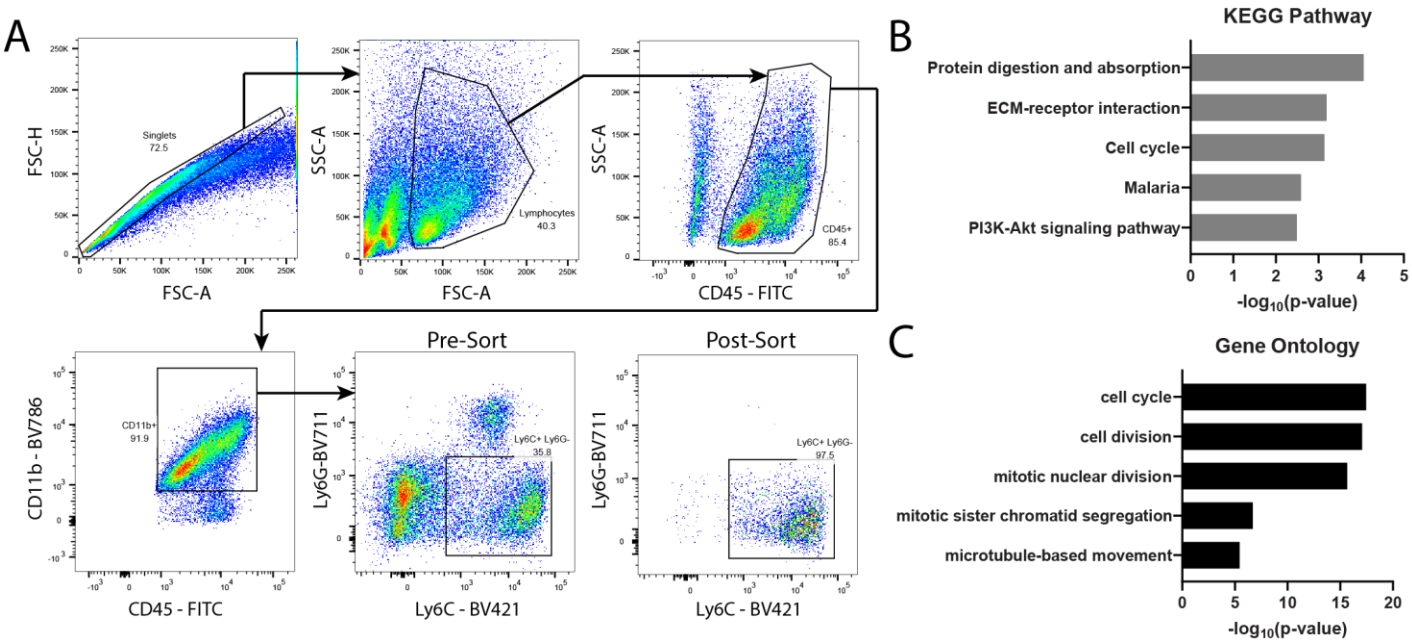

Supplemental Figure 9. Monocytes from the CNS of mice with EAE treated with anti-CSF-1 MAb have distinct transcriptional profile. EAE was induced in C57BL/6J mice by immunization with MOG_{35-55}. Mice were treated with 200 μg/day of anti-CSF-1 MAb or isotype control MAb from day 11 to 16 p.i. and sacrificed on day 17 p.i. **A)** Gating strategy for FACS sorting of CD45^{Hi}CD11b⁺Ly6G⁻Ly6C⁺ monocytes/monocyte-derived cells. **B)** Gene ontology and **C)** KEGG pathway terms ranked by significance and generated from differentially expressed genes between monocytes/monocyte derived cells from anti-CSF-1- and isotype control MAb-treated mice.

Supplemental Figure 10

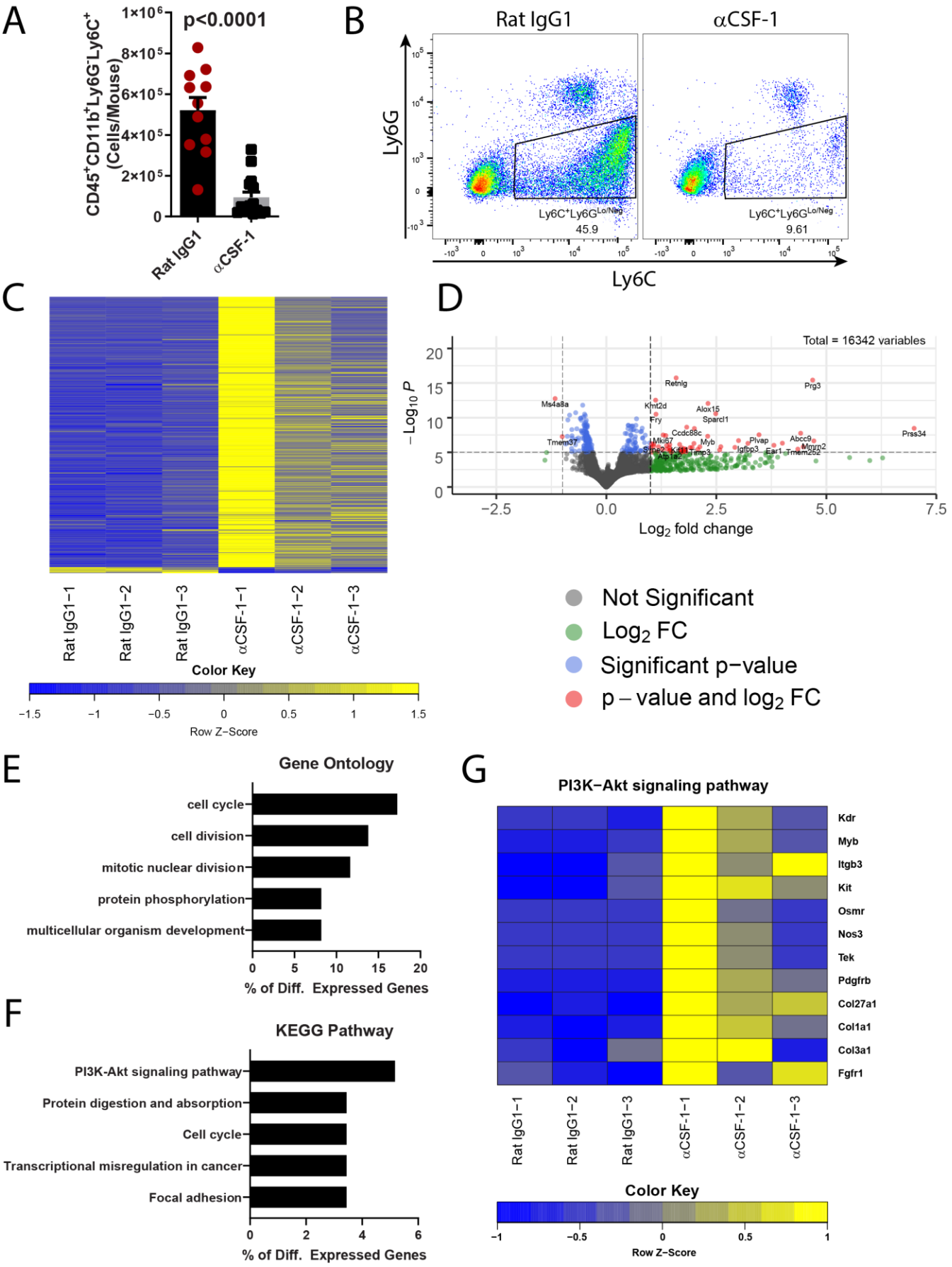

Supplemental Figure 10. Monocytes from the CNS of anti-CSF-1 MAb-treated mice with EAE have a transcriptionally distinct phenotype. EAE was induced in C57BL/6J mice by immunization with MOG_{35-55}. Mice were treated with 200 μg/day of anti-CSF-1 MAb or isotype IgG1 control MAb (n=3/group) from day 11 to 16 p.i. and sacrificed on day 17 p.i. **A)** Numbers of $CD45^{Hi}CD11b^{+}Ly6G^{-}Ly6C^{+}$ monocytes. **B)** Flow cytometry plots showing expression of Ly6C and Ly6G among $CD45^{+}CD11b^{+}$ cells. **C)** Heatmap showing differentially expressed transcripts in monocytes from anti-CSF-1- and isotype MAb-treated mice. Criteria for inclusion in heatmap were expression in all samples, with a p-adjusted value < 0.05 and a $\log_2$ fold change greater/less than ±1. **D)** Volcano plot showing relative expression of transcripts detected in samples from anti-CSF-1- and isotype MAb-treated mice. **E)** Gene ontology and **F)** KEGG pathway terms that were significantly enriched (p<0.05) and ranked by percentage of differentially expressed genes (p-adj<0.01). **G)** Heatmap of z-score- normalized TPM data from differentially expressed genes detected from the PI3K-Akt signaling pathway KEGG term.

Supplemental Figure 11

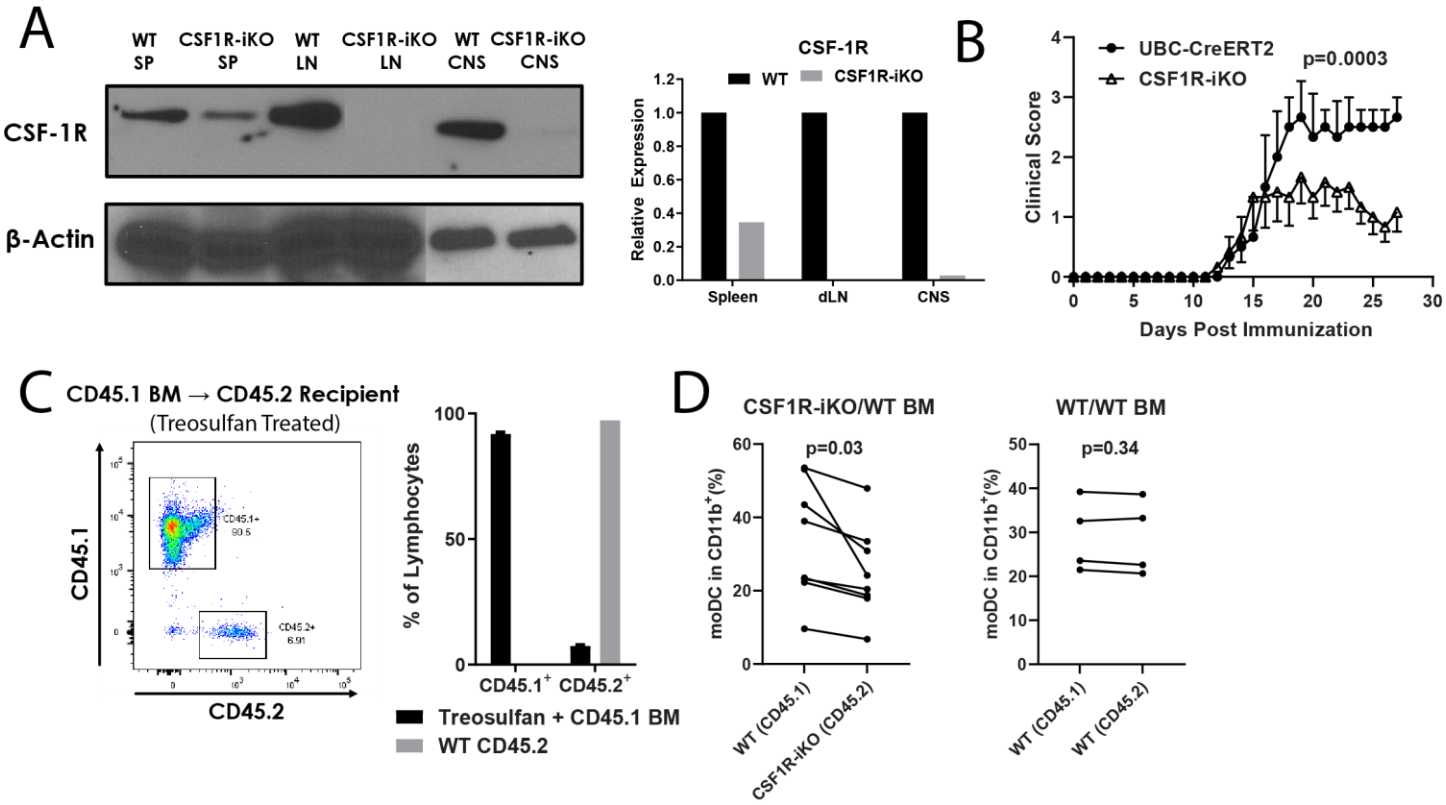

Supplemental Figure 11. High degree of chimerism in treosulfan-induced BM chimera mice; and reduction of moDCs in CSF1R-iKO/WT mixed BM chimeras. A) Western blot showing protein level of CSF-1R in cell lysates of whole spleen, draining lymph nodes, and CNS mononuclear cells 5 days after 5-day treatment with tamoxifen. Relative expression, shown in the right panel, was calculated by densitometry of CSF-1R signal relative to β-actin signal, then normalized to WT expression. Each bar represents pooled lysate from 5 mice, with equal numbers of cells from each mouse pooled together. **B)** EAE in tamoxifen-treated CSF1R-iKO (n=6) and UBC-CreERT2 (n=3) mice. Significance was determined by two-way ANOVA. **C)** WT $CD45.2^{+}$ recipient mice were treated with treosulfan and rested for 72 h, then reconstituted with 10^{7} BM cells from $CD45.1^{+}$ mice. After 32 days, blood was collected via tail vein and reconstitution efficiency determined. Left panel shows flow cytometry plot of CD45.1 and CD45.2 expression in PBMCs. Right panel shows quantification of reconstitution efficiency. WT CD45.2 (grey bar) represents blood from naïve WT $CD45.2^{+}$ mice. **D)** Quantification of $CD45^{+}SalI1^{-}CD11b^{+}Ly6G^{-}CD11c^{+}Ly6C^{+}MHCII^{+}$ moDCs in mixed BM chimeras. Left panel shows moDCs in the CNS from mice reconstituted with a 1:1 mixture of WT and CSF1R-iKO BM cells. Right panel shows moDCs from mice reconstituted with a 1:1 mixture of CD45.1 WT and CD45.2 WT BM cells. moDCs derived from CD45.1 and CD45.2 immune cells in the CNS were compared. Significance was determined by paired *t* test.